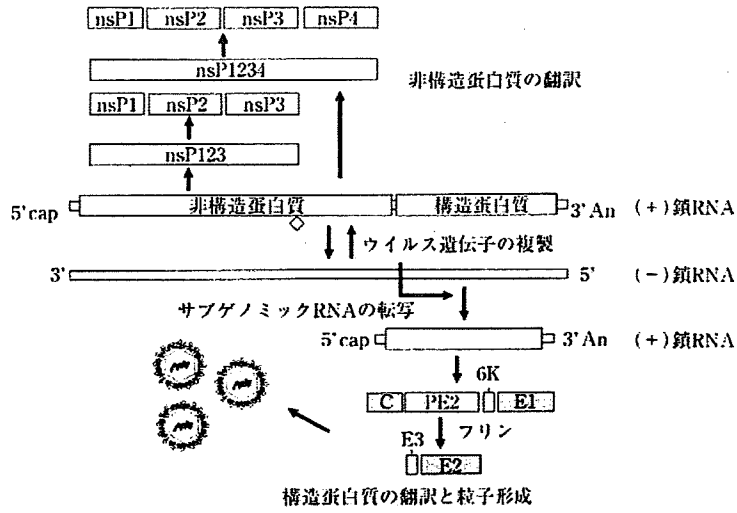

図3　アルファウイルスの遺伝子構造

中央にウイルスRNAを示す．非構造蛋白質の翻訳過程を上部に構造蛋白質の翻訳過程を下部に記す．◇はオパール終止コドン（UGA）を示す．いくつかのチクングニヤウイルス株のゲノムにはnsP4の数コドン前にオパールコドンが存在し，オパールコドンを読み飛ばすことにより2種のポリ蛋白質（P123とP1234）が形成される．構造蛋白質はサブゲノミックRNAより翻訳される．また成熟ウイルス粒子に取り込まれる蛋白質を□で示す．

報告され，さらに219人の死者が報告された[1,3]．

2. 南アジアおよび東南アジア

1954年以来フィリピン，タイ，カンボジア，ベトナム，ラオス，マレーシア，インドネシア，ミャンマー，スリランカ，インド等のアジア諸国ではチクングニヤ熱の流行がたびたび報告されている[3]．フィリピンでは1954～1986年に流行が報告された．タイでは1958年に最初の流行が報告され，1962年には推計4万人の患者が人口200万人の都市部で報告された．スリランカでは血清学的調査により1960年に初めてチクングニヤウイルス感染が確認され，1965～1966年に推計163,000人の患者が報告された．インドでは1963年にコルカタで最初のチクングニヤ熱の流行が報告され，158人の死亡が記録されている．さらに1964年のチェンナイでの流行では40万人近くの症例が記録されている．

近年，南アジアおよび東南アジアにおいて再びチクングニヤ熱が大流行している．インドでは2005～2006年に少なくとも140万人の症例が報告されている[3]．流行はスリランカに拡大し2006年10月から2008年6月にかけてチクングニヤ熱患者が推計4万人報告された．さらに流行は東南アジアに拡散し，シンガポール，マレーシア，タイでの流行が確認されている．シンガポールでは2007年12月まで主にインドからの輸入症例が散発していたが，2008年1月に国内症例が初めて報告され，2009年2月までに900例以上の患者が報告されている．またマレーシアでも2009年2月までに4,000症例以上の患者が報告されている．さらにタイでもタイ南部を中心に2008年～2009年2月の間に10,500例以上の患者が報告されている．

3. 輸入症例とイタリアでの流行

近年の流行ではヨーロッパ，米国，カナダ，仏領ギアナ，オーストラリア，シンガポール，マレーシア，香港，台湾，日本において輸入症例が報告されている[3-5]．2005～2006年には約800例の

輸入症例がフランスにおいて報告されており，そのほとんどがインド洋諸島からである[6]．ドイツ，イタリア，イギリス，ノルウェー，オランダ，ベルギー，チェコ，スイス等の他のヨーロッパ諸国でもインド洋諸島および南アジアからの輸入症例が報告されている．ヨーロッパ，北中米，オーストラリア，東アジアにおいてもチクングニヤウイルスの媒介蚊であるヒトスジシマカが生息しており，これら地域でチクングニヤ熱が流行する可能性は否定できない[3]．事実イタリア北東部では2007年7月4日から9月27日の間に205人（死者1人）の患者が報告された[7]．イタリアの流行ではヒトスジシマカからもウイルス遺伝子が検出された．疫学的解析の結果イタリアでの流行はインドからの訪問者による輸入症例から流行が始まったと考えられている．

■チクングニヤウイルスの生態

チクングニヤウイルスは自然宿主であるヒトやサルとカの間で感染環を形成・維持している．主要な媒介蚊はシマカ属のカである．感染環は森林型，都市型に分けられる．森林型はアフリカで確認されており散発的流行の原因となっている．ギニヤヒヒ（*Papio papio*）等の霊長類，リス等の齧歯類，コウモリ等の翼手類とカの間で感染環が維持されている．森林型を媒介する主な媒介蚊はアフリカでは*A. furcifer*等である[3]．都市型はヒトとカの間で感染環が成立した流行型である．都市型サイクルを媒介する主要な媒介蚊はアフリカ，アジアいずれの流行地域でもネッタイシマカおよびヒトスジシマカである．ネッタイシマカは熱帯地域に広く分布する主な媒介蚊である．近年のレユニオン島およびイタリアの流行はヒトスジシマカの媒介によるものである[3]．急性期のヒトにおけるウイルス血症は非常に高く，この時期に吸血したカが感染する可能性はきわめて高い．したがって温帯地域においても輸入症例からチクングニヤウイルスが侵入する可能性は否定できない．また特殊な感染経路として実験室内感染も報告されているため医療関係者，研究関係者は特に注意が必要である．

■臨床像

チクングニヤウイルスの潜伏期間は2～12日で，多くは不顕性感染に終わるが，チクングニヤ熱を発症すると発熱，全身倦怠，リンパ節腫脹，頭痛，筋肉痛，発疹，亜急性の関節炎を呈する[4]．発熱は39～40℃に達し，間欠性の悪寒を伴う．また出血傾向（鼻出血・歯肉出血）や悪心・嘔吐，腫脹，末梢リンパ節症，羞明，無力症をきたすこともある．ほとんどの症状は3～10日で消失するが関節炎は数週間から数カ月持続する．関節炎は特に指関節，手根関節，膝関節，足関節に多発し，持続する場合，激しい関節痛および多発性腱滑膜炎を伴う慢性末梢性リューマチ様症状を呈するため日常生活に困難を伴う．主な血液所見はリンパ球減少および血小板減少であり，ALT，ASTの上昇も認められる．フランスでの47例の輸入症例では80%の患者に10病日後も日常生活に支障をきたす関節痛が認められ，6%の患者が入院した[7]．発症2日後までは高いウイルス血症が観察され，2～3日後には低下し，6日後には消失した．中和抗体は5病日から検出された．ところで近年のレユニオン島での流行では213例の死亡例が，特に75歳以上の高齢者において報告されたが，これらの例では呼吸器不全，心代償不全，髄膜脳炎，劇症肝炎，腎不全等が報告されている[3]．

■診断法

臨床診断においてチクングニヤ熱に特徴的な症状である発熱，リューマチ様症状あるいは発疹などを認めた場合はこの疾患を疑うべきである．またチクングニヤウイルスの日本への侵入は現在まで認められていないためウイルス侵淫地域を2週間以内に訪問した経歴があること，またはこの地域からの訪問者であること等の確認が重要である．急性期および慢性期の関節炎は関節リューマチとの鑑別が困難である．チクングニヤ熱の臨床症状

はデング熱との鑑別が必要である．媒介蚊を共有するためアフリカ，アジアにおける分布域もほぼ一致する．デング熱では関節痛よりも筋肉痛が主であり，デング出血熱ではショック症状が認められることがある．チクングニヤ熱の確定診断には実験室診断が必須である．確定診断には病原体検査と血清学的検査が行われる．前者は血清からのウイルス分離あるいはウイルス遺伝子の検出を目的とし，後者はIgM捕捉ELISA，中和抗体試験，HI試験等による抗ウイルス抗体の検出を目的とする．ウイルス分離は急性期患者の血清，血漿を用いて乳のみマウスの脳内接種，動物細胞(Vero，BHK-21細胞等）および昆虫由来培養細胞(C6/36細胞等）への接種，カの胸部接種にて行う．ウイルス遺伝子の検出にはRT-PCR法，リアルタイムPCR法を用いる．ウイルス遺伝子は患者の血清，血漿より精製し，RT-PCR法，リアルタイムPCR法に供試して，陽性および陰性コントロールを基準に目的領域の特異的増幅を確認する．血清学的検査は抗ウイルス抗体の検出を目的とする．IgM抗体捕足ELISAは感度・特異性が高い検査法である．IgM抗体は発症後3～6カ月間検出可能である．中和抗体は感染5～7病日に上昇が認められるが，急性期（発病後5日以内）および回復期（発病後14日以上）のペア血清を用いた中和試験により4倍以上の抗体価上昇を確認すべきである．プラーク法による中和試験はVero細胞を用いて50%プラーク減少法により行う．またその他の鑑別疾患として他のアルファウイルスあるいはマラリア等の熱性疾患に留意する必要がある．

■治　療

現在チクングニヤ熱に対する特異的治療法は確立されていないため，対症療法が中心である．また感染により終生免疫が獲得されると考えられている．治療にあたってはデング熱あるいはマラリア等の感染症でないことを確認することが重要である．また急性期においては感染環を遮断するために媒介蚊と患者の隔離にも注意する．起床時の関節痛は体を動かすことにより改善することがあるが，激しい運動では症状が悪化する．抗炎症剤あるいは鎮静剤により関節痛は改善するが，顕著な効果が認められず回復に数カ月を要した症例も報告されている[9]．またインターフェロンαとribavirinの併用による抗ウイルス効果がVero細胞を用いた*in vitro*において報告されているが，臨床的応用の報告はない[3]．

■予防法

ワクチンは実用化されていない．したがってチクングニヤウイルスの侵淫地域においては感染するリスクを減らすため，媒介蚊に刺されることを避けることが重要である．そのためにはカの吸血時間帯である夕方から夜明けにかけての野外活動を避ける，肌の露出を避ける，N,N-diethyl-3-methylbenzamide（DEET：ディート）等を含む忌避剤を使用する等の対策が必要である．忌避剤の有効成分の濃度が高いほど効果が持続するが，濃度による効果の差はない．流行地域への渡航者は特に注意が必要である．長期滞在者は媒介蚊の防除・駆除および媒介蚊の繁殖を抑制することが必要である．家屋では媒介蚊の侵入を防ぐスクリーン（網）等を設置する等の対策をとる．感染拡大を防ぐためには媒介蚊の発生源となる溜まり水の除去，花瓶等の適切な管理を行うことも重要である．地域社会においては媒介蚊の繁殖可能な古タイヤ等の廃棄物の除去，屋外イベントでの忌避剤使用の奨励などが必要となる．流行地における滞在によりチクングニヤウイルス感染が疑われた場合は速やかに信頼できる医療機関を受診するとともに感染拡大を防ぐために媒介蚊との接触に注意する必要がある．

チクングニヤウイルス対策においてワクチン開発は最も有効な対策の1つである．チクングニヤウイルスは世界の広い地域に分布しているにもかかわらず，それぞれのウイルス株は血清学的に交差するため多くの株間に有効なワクチンが開発可

能である．近年の世界におけるチクングニヤ熱の爆発的な流行あるいは実験室内感染者の報告等により，安全で効果的なワクチンが望まれる．これまでに①タイ 15561 株を用いたホルマリン不活化ワクチン，②タイ 15561 株を MRC-5 細胞（ヒト胎児肺細胞）で継代して得た CHIK 181/Clone 25 株を用いた弱毒生ワクチン TSI-GSD-218 株開発が報告されている．不活化ワクチンは 16 人のボランティアに 4 週間隔で 2 回免疫された．その結果すべての被験者において十分な免疫応答が観察され，副反応は報告されていない[7]．弱毒生ワクチンは第Ⅱ相試験（～10^5pfu/ドーズ）が行われ，14 日以内に被験者 40 人（69%），28 日以内に 57 人（98%）で抗体の上昇が観察された．ただし 5 人（8%）の被験者において一過性の関節痛が報告された．12 カ月後では 85%の被験者において中和抗体の維持が確認された[8]．

■感染症法における取扱い

チクングニヤ熱は「感染症の予防および感染症の患者に対する医療に関する法律」（感染症法）および検疫法に指定されていない．確定診断のための検査は国立感染症研究所ウイルス第一部において実施可能である．

■おわりに

多くの輸入症例がアジア，ヨーロッパ，アメリカで報告されている．さらに 2006～2009 年には日本において 5 例の輸入症例が報告された．これらの輸入症例患者の渡航先は流行地であるインド，スリランカ，インドネシア，マレーシアであった．現在も南アジア，東南アジアでは流行が継続していることから，流行地域への渡航者に対する注意喚起がいっそう重要である．急速な輸送手段の発達とネッタイシマカ，ヒトスジシマカの分布拡大，熱帯雨林地域での人口拡張により世界の熱帯・亜熱帯地域においてチクングニヤ熱は今後も流行が続くことが予想される．治療法は確立されておらず，チクングニヤ熱の流行にはヒト，カ，気候，環境等の要因が複雑にかかわり，その状況の予測は困難である．媒介蚊の生息する日本へのチクングニヤウイルスの侵入は予断を許さない．熱帯・亜熱帯地域からの帰国者の関節痛あるいは筋肉痛を伴う発熱疾患においてはデング熱，デング出血熱とともに本疾病を考慮に入れる必要がある．現在，チクングニヤウイルスに関する知見が収積されつつあり，国内においても国立感染症研究所等いくつかのウェブページ等を通じてチクングニヤウイルスの情報が提供されている（例えば http://www.nih.go.jp/vir1/NVL/NVL.html）．旅行者は旅行先におけるチクングニヤ熱の流行状況を把握し，蚊対策に十分考慮することが必要である．

謝　辞　稿を終えるにあたり，ご校閲を賜りました国立感染症研究所ウイルス第一部倉根一郎部長および高崎智彦第二室長に深謝申し上げます．本論文の一部のデータは厚生労働科学研究費補助金（新興・再興感染症研究事業）（H19－新興－一般－003）によって得られたものである．

1) WHO：Outbreak and spread of chikungunya. *Wkly Epidemiol Rec* 82：409-415, 2007.
2) Strauss JH, Strauss EG：The alphaviruses：gene expression, replication, and evolution. *Microbiol Rev* 58：491-562, 1994.
3) 林　昌宏：チクングニヤ熱．化学療法の領域 24：1606-1613, 2008.
4) 水野泰孝，加藤康幸，工藤宏一郎ほか：遷延する関節痛より確定診断に至ったチクングニヤ熱の本邦初症例．感染症学雑誌 81：600-601, 2007.
5) 青山幾子，弓指孝博，加瀬哲男ほか：チクングニヤ熱と確定診断されたインドからの輸入感染症症例．病原体微生物検出情報 29：345-346, 2008.
6) Simon F, Parola P, Grandadam M *et al.*：Chikungunya infection：an emerging rheumatism among travelers returned from Indian Ocean islands. Report of 47 cases. *Medicine* 86：123-137, 2007.
7) Harrison VR, Eckels KH, Bartelloni PJ *et al.*：Production and evaluation of a formalin-killed Chikungunya vaccine. *J Immunol* 107：643-647, 1971.
8) Levitt NH, Ramsburg HH, Hasty SE *et al.*：Development of an attenuated strain of chikungunya virus for use in vaccine production. *Vaccine* 4：157-162, 1986.

JOURNAL OF VIROLOGY, Nov. 2009, p. 11133–11141 Vol. 83, No. 21
0022-538X/09/$12.00 doi:10.1128/JVI.00959-09

Two-Step Conformational Changes in a Coronavirus Envelope Glycoprotein Mediated by Receptor Binding and Proteolysis▽

Shutoku Matsuyama* and Fumihiro Taguchi†

Department of Virology III, National Institute of Infectious Diseases, 4-7-1 Gakuen Musashi-Murayama, Tokyo 208-0011, Japan

Received 14 May 2009/Accepted 4 August 2009

The coronaviruses mouse hepatitis virus type 2 (MHV-2) and severe acute respiratory syndrome coronavirus (SARS-CoV) utilize proteases to enter host cells. Upon receptor binding, the spike (S) proteins of both viruses are activated for membrane fusion by proteases, such as trypsin, present in the environment, facilitating virus entry from the cell surface. In contrast, in the absence of extracellular proteases, these viruses can enter cells via an endosomal pathway and utilize endosomal cathepsins for S protein activation. We demonstrate that the MHV-2 S protein uses multistep conformational changes for membrane fusion. After interaction with a soluble form of the MHV receptor (CEACAM1a), the metastable form of S protein is converted to a stable trimer, as revealed by mildly denaturing sodium dodecyl sulfate-polyacrylamide gel electrophoresis. Liposome-binding assays indicate that the receptor-bound virions are associated with the target membrane through hydrophobic interactions. The exposure of receptor-bound S protein to trypsin or cathepsin L (CPL) induces the formation of six-helix bundles (6HB), the final conformation. This trypsin- or CPL-mediated conversion to 6HB can be blocked by a heptad repeat peptide known to block the formation of 6HB. Although trypsin treatment enabled receptor-bound MHV-2 to enter from the cell surface, CPL failed to do so. Interestingly, consecutive treatment with CPL and then chlorpromazine enabled a portion of the virus to enter from cell surface. These results suggest that trypsin suffices for the induction of membrane fusion of receptor-primed S protein, but an additional unidentified cellular factor is required to trigger membrane fusion by CPL.

Enveloped viruses enter cells through fusion of their envelope with the cellular membrane. A number of enveloped viruses utilize proteases to activate their surface glycoproteins for fusion. There are two major mechanisms for protease activation of viral glycoproteins. For many viruses, such as human immunodeficiency virus, influenza virus, and Nipah virus, the protease (e.g., furin, trypsin, or cathepsin) makes a simple proteolytic cut in the glycoprotein during biogenesis, separating the receptor-binding and fusion subunits. This cleavage converts the precursor glycoprotein to its fusion-competent state, which is presented on the virion surface. Alternatively, for other viruses such as ebolavirus and severe acute respiratory syndrome coronavirus (SARS-CoV), the proteases cleave the viral glycoprotein and induce its conformational changes during viral entry, following receptor binding and/or endocytosis (5, 13, 20, 23). However, the mechanism underlying this second situation has not been fully characterized.

The 200-kDa spike (S) proteins of murine coronavirus mouse hepatitis viruses (MHV) are class I fusion proteins that are generally cleaved into S1 and S2 subunits by cellular proteases during biogenesis. The N-terminal S1 subunit forms the surface knoblike structure of the spike, which is responsible for receptor binding, and the C-terminal membrane-anchored S2 subunit forms the stem, which is important for virus-cell membrane fusion (4). Similar to the S protein of SARS-CoV, the S protein of MHV type 2 (MHV-2) is not cleaved during biogenesis. However, regions corresponding to S1 and S2 are retained in these molecules.

The conformational changes of MHV-2 and SARS-CoV S proteins are thought to be similar to the class I fusion proteins human immunodeficiency virus GP160, influenza hemagglutinin (HA), and other coronaviral S proteins. One of the most important features of the protein is the conserved heptad repeat (HR) regions (HR-C and HR-N), which play an essential role in virus-cell fusion activities. In the fusion process, HR-N forms an interior trimeric coiled-coil structure to which the three HR-Cs bind in an antiparallel fashion, resulting in the formation of a six-helix bundle (6HB). This structure brings viral and cellular membranes into close proximity to facilitate membrane fusion. Synthetic short peptides corresponding to the HR (HR-P) regions of class-I fusion proteins have been shown to block the interaction of HR-N and HR-C complexes, resulting in the inhibition of a number of viral infections (27).

In the entry of SARS-CoV, Simmons et al. reported that two steps of conformational changes are necessary for final invasion of cells (22). The first step takes place after binding to the receptor, and the subsequent step is driven by cleavage of the S protein by protease. This mechanism was predicted by studies of viral infection using intervirion interactions; however, structural analyses of the conformational changes of S protein were not performed. In the present study, we examined the conformational changes of MHV-2 S in terms of the structural changes and revealed that, in agreement with the findings for SARS-CoV, MHV-2 S also requires at least two steps of conformational changes for fusion triggering. However, the last stage of MHV-2 entry, envelope-endosome membrane fusion, seems to be different from that of SARS-CoV. SARS-CoV

* Corresponding author. Mailing address: Department of Virology III, National Institute of Infectious Diseases, 4-7-1 Gakuen Musashi-Murayama, Tokyo 208-0011, Japan. Phone: 81-42-561-0771, ext. 3755. Fax: 81-42-567-5631. E-mail: matuyama@nih.go.jp.

† Present address: Nippon Veterinary and Life Science University, 1-7-1 Sakai-minami, Musashino, Tokyo 180-8602, Japan.

▽ Published ahead of print on 12 August 2009.

entry from endosomes can be facilitated by cathepsin L (CPL) alone (3, 22), while another unidentified factor together with CPL is probably critical for the final virus-endosome membrane fusion of MHV-2. We propose a possible mechanism for the entry of MHV-2, which may also be utilized by other enveloped viruses that require endosomal cathepsins.

MATERIALS AND METHODS

Cells, viruses, and soMHVR. DBT cells was maintained in Dulbecco modified Eagle medium (DMEM) low glucose (Gibco) supplemented with 5% fetal bovine serum. MHV-2 was propagated in DBT cells as previously reported, and the supernatants of culture fluids, DMEM containing 10% tryptose phosphate broth (Difco), were used for experiments. The soluble MHV receptor (soMHVR) was produced by using a recombinant baculovirus and purified as previously described (12).

Western blot analysis. MHV-2 S protein was analyzed by Western blotting as described previously (12). Briefly, each sample was boiled with sample buffer containing 0.5% sodium dodecyl sulfate (SDS), separated by using a 3 to 10% gradient gel with 0.1% SDS (SDS-polyacrylamide gel electrophoresis), and transferred to a membrane. S proteins on the membrane were reacted with anti-S1 (11F) and anti-S2 (10G) monoclonal antibodies (MAbs) (21) or anti-S2A (25) and subsequently with anti-mouse (for 11F and 10G) or anti-rabbit (for anti-S2A) immunoglobulin G labeled with horseradish peroxidase.

S protein oligomer assay. The step 1 conformational changes of S protein were detected by mildly denaturing SDS-PAGE. A 9-μl portion of MHV-2 was mixed with 1 μl (10 μg/ml) of soMHVR (12). For step 1 incubations, samples were warmed to 37°C for 20 min, treated with sample buffer containing 0.1% SDS, and incubated for 5 min at room temperature. Samples were analyzed by Western blotting as described above.

Proteinase K digestion assay. The step 2 conformational changes of the S protein were examined by a proteinase digestion assay as previously described (12). MHV-2 and soMHVR were mixed and incubated as described above. For two-step incubations, samples were adjusted to pH 7.4 or 5.0 with 40 mM HEPES–40 mM MES (morpholineethanesulfonic acid) and mixed with 1 μg of trypsin/ml or 18 μg of CPL (Calbiochem)/ml. After a 20-min incubation at 37°C, 1 μl of 1 M Tris (pH 8.0) was added to neutralize low-pH-treated samples, and samples were treated with 1 μg of proteinase K/ml at 4°C for 20 min. The digested S proteins were analyzed by Western blotting as described above.

Liposome-binding assay. Lipids, L-phosphatidylcholine (PC; egg; Avanti-Polar Lipids), L-phosphatidylethanolamine (PE; egg; Avanti-Polar Lipids), sphingomyelin (Sph; brain; Avanti-Polar Lipids), and cholesterol (Chol; Sigma Chemical Co.) were mixed in a 1:1:1:1.5 molar PC-PE-Sph-Chol ratio, dried under N_2 gas in a glass tube, and lyophilized overnight. After the addition of phosphate-buffered saline (pH 7.2; PBS), the lipid suspension was vortexed and then extruded 25 times through a 0.4-μm-pore-size Nuclepore filter in an Avanti-Mini-Extruder. Liposomes (5.6 mM lipid on the basis of the input lipid) were stored at 4°C and used within 1 week. A liposome-binding assay was performed as described previously (6, 28), with minor modifications. Then, 4 μl of MHV-2 and 15 μl of liposomes were incubated with 1 μM soMHVR in a final volume of 20 μl of PBS at 37°C for 20 min. The samples were overlaid on a discontinuous sucrose gradient consisting of 300 μl of 20% sucrose, 300 μl of 30% sucrose, and 30 μl of 40% sucrose in a 700-μl Ultra-Clear centrifuge tube (Beckman). After centrifugation at 40,000 rpm for 1 h at 4°C, 200-, 250-, and 200-μl fractions were drawn from the air-fluid interface. Viral RNAs were isolated from the fractions with the addition of an equal volume of Isogen (Nippon Gene), and 50 μg of yeast tRNA (Sigma) was added as a carrier. Samples were then subjected to real-time PCR to quantify the amount of genomic RNA as described below.

Virus entry assay. DBT cells in 96-well culture plates were treated with DMEM containing 200 μM bafilomycin A1 (DMEM+Baf) at 37°C for 30 min and then chilled on ice for 10 min. Approximately 10^5 PFU of virus in DMEM+Baf was used to infect 10^5 cells on ice. After a 30-min adsorption, the virus was removed, and infected cells were treated for 10 min with various concentrations of proteases in DMEM+Baf prewarmed to room temperature. Trypsin was used as a positive control for inducing fusion at the plasma membrane. After the protease was removed, the cells were cultured in DMEM+Baf at 37°C for 5 h. Viral RNAs were isolated from cells with the addition of 200 μl of Isogen. Real-time PCR was performed to estimate the amounts of newly synthesized mRNA7 as described below.

Quantitative estimation of viral RNA by real-time PCR. Real-time reverse transcription-PCR to estimate the amount of viral RNA was performed as described previously for SARS-CoV mRNA detection (13), with slight modifications for MHV-2 detection. To quantify the amounts of mRNA7, the target sequence was set at the inside of MHV-2 N gene. To detect the amplified fragments, we used hybridization probes labeled with fluorescent dye, 5′-GCTC CTCTGGAAACCGCGCTGGTAATGG-3′ (3′ fluorescein isothiocyanate labeled) and 5′-ATCCTCAAGAAGACCACTTGGGCTGACCAAACC-3′ (5′ LCRed640 labeled). For amplification of the fragment from viral RNA, we used the pair of oligonucleotides 5′-TGTCTTTTGTTCCTGGGCA-3′ (MHV-2 mRNA7 forward) and 5′-CAAGAGTAATGGGGAACCA-3′ (MHV-2 mRNA7 reverse). Finally, for amplification of the fragment from mRNA7, we used the pair of oligonucleotides 5′-GTACGTACCCTTTCTACTC-3′ (MHV-2 leader) and 5′-CAAGAGTAATGGGGAACCA-3′ (MHV-2 mRNA7 reverse). These oligonucleotides were synthesized according to the MHV-2 N gene sequence. PCR analysis was performed under the following conditions (room temperature, 61°C for 20 min; PCR, 95°C for 30 s; 40 cycles for 95°C for 5 s, 55°C for 15 s, and 72°C for 13 s). The amount of virus in cells was calculated from the calibration line as described previously (13).

RESULTS

The first step in conformational change in the MHV S protein is induced by receptor binding. To visualize the first step in conformational changes in MHV-2 S, an S protein oligomer assay was performed using two S2-specific antibodies: MAb 10G, which recognizes HR-C, and anti-S2A, which is antiserum produced by immunizing rabbits with a synthetic peptide that encompasses the S2A epitope and recognizes the region near the fusion peptide (19, 25), as depicted in Fig. 1A. As shown in Fig. 1B, a major band at 200 kDa, as well as 380-kDa and 500-kDa bands, was detected by MAb 10G when the virus was incubated without soMHVR (Fig. 1B, lane 3). When the virus was incubated with increasing concentrations of soMHVR, the major band was shifted to 500 kDa in a concentration-dependent manner (lane 4 to 7). This 500-kDa band is thought to be a trimer of the S protein induced by soMHVR. The dimer and trimer formations of S protein detected by SDS-PAGE were also reported in a study of SARS-CoV (24), as was dimerization of S1 subunits by receptor binding in a study of MHV (10). For SARS-CoV, the major band of S protein was detected as a stable trimer without receptor interaction. However, in the present study, the MHV-2 S protein exhibited a trimer band whose mobility is similar to the SARS-CoV S trimer only after interaction with soMHVR. Furthermore, boiling the sample failed to reduce the amount of the 500-kDa band, suggesting that the trimerization is established in a stable manner (lane 2). Interestingly, the anti-S2A antibody detected the 500-kDa band in unboiled samples (lanes 10 to 14) but not in boiled samples. This indicates that S2A recognizes native S protein that has undergone conformational changes exposing the fusion peptide after binding to soMHVR. These results collectively suggest that the MHV-2 S protein undergoes step 1 conformational changes after interaction with soMHVR, from the metastable form to a stable trimer, which results in the exposure of the fusion peptide. Furthermore, since the conformational changes of srr7 S protein have been well documented (12), we compared the MHV-2 S trimer to the cleaved type S protein bearing the MHV-JHM-srr7 and found that soMHVR induced its 6HB. As shown in Fig. 1C, soMHVR induced the formation of an 85-kDa srr7 S2 subunit reactive to the MAb 10G but failed to induce a trimer (lane 4). This result suggests that the srr7 S protein is not arrested at the intermediate stage as a trimer after receptor binding.

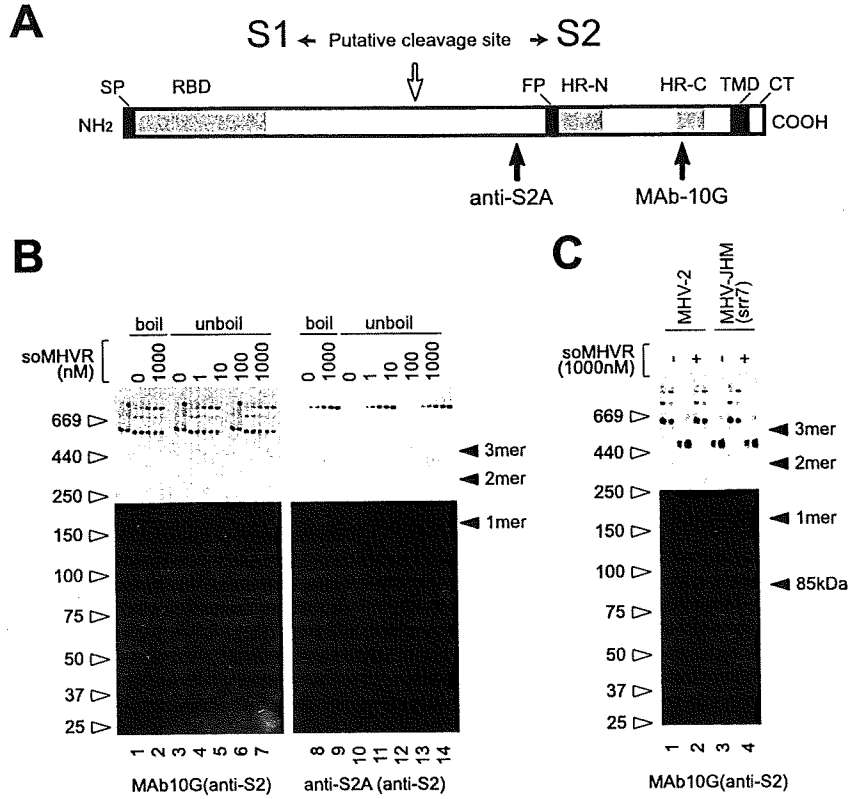

FIG. 1. Schematic structure and step 1 conformational change of MHV-2 S protein induced by receptor binding. (A) The S protein has an N-terminal signal peptide (SP), a receptor-binding domain (RBD), a fusion peptide (FP), two heptad repeats (HR-N and HR-C), a transmembrane domain (TMD), and a cytoplasmic tail (CT). The putative cleavage site in the central region is identified by a white arrow. Epitopes recognized by the two antibodies (MAb 10G and anti-S2A) are depicted. (B) MHV-2 virions were incubated with various concentrations of soMHVR at 37°C for 30 min. The samples were boiled (lanes 1, 2, 8, and 10) or left unboiled (lanes 3 to 7 and lanes 10 to 14) and analyzed by Western blotting with the indicated antibody. (C) Precleaved and uncleaved S proteins of MHV-JHM-srr7 and MHV-2 were incubated in the presence or absence of soMHVR to compare the trimer formation. The samples were analyzed by native PAGE and Western blotting with the indicated antibody.

Binding of S protein to soMHVR facilitates the interaction of MHV with liposomes. We next examined whether the fusion peptide in S protein interacts with target membranes by using a liposome binding assay. We first tried to detect liposome binding of the virions by Western blotting, as has been done with other viruses (6, 28), but we could not detect virus binding. We therefore performed this binding assay using real time-PCR, which is more sensitive at detecting a small amount of virus. In this assay, virus and liposomes are mixed in the presence or absence of receptor, overlaid on a sucrose step gradient, and centrifuged. If the virus binds the liposomes, it floats to the top of the gradient with the liposomes (28). Otherwise, it is precipitated at the bottom of the tube. As shown in Fig. 2, in the absence of receptor the majority of the viral RNA was detected in the bottom fraction, and only a small amount was detected in the middle and top fractions. However, incubation of MHV-2 with soMHVR and liposomes resulted in high co-localization of MHV-2 with the liposomes in the top fraction of the gradient. This figure is shown in a log scale and implies that ca. 50% of the virus was attached to the liposomes. This value is not unexpectedly low since some coronaviruses contain a few projections of S protein that could fail to bind soMHVR. Together with the result shown in Fig. 1B, this indicates that the interaction of MHVR with MHV-2 S protein induces con-

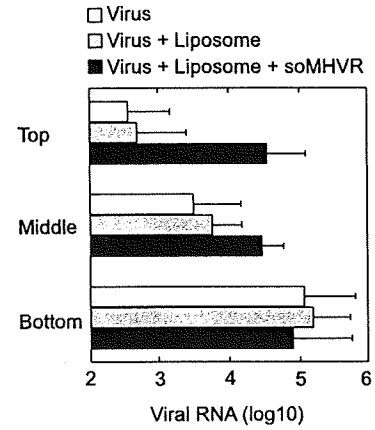

FIG. 2. Hydrophobic interactions of receptor-primed MHV-2 with liposome. Virions incubated in the absence of liposomes and soMHVR (□) or in the presence of liposomes only (▨) or both liposomes and soMHVR (■) were overlaid onto the top fraction of a step gradient and spun at 40,000 rpm for 1 h. The top, middle, and bottom fractions were drawn from the air-fluid interface, and viral RNAs were isolated from the fractions. Viral genomic RNA was quantified by real-time RT-PCR. The vertical line extending to the right of the bar indicates the standard deviation of four different experiments.

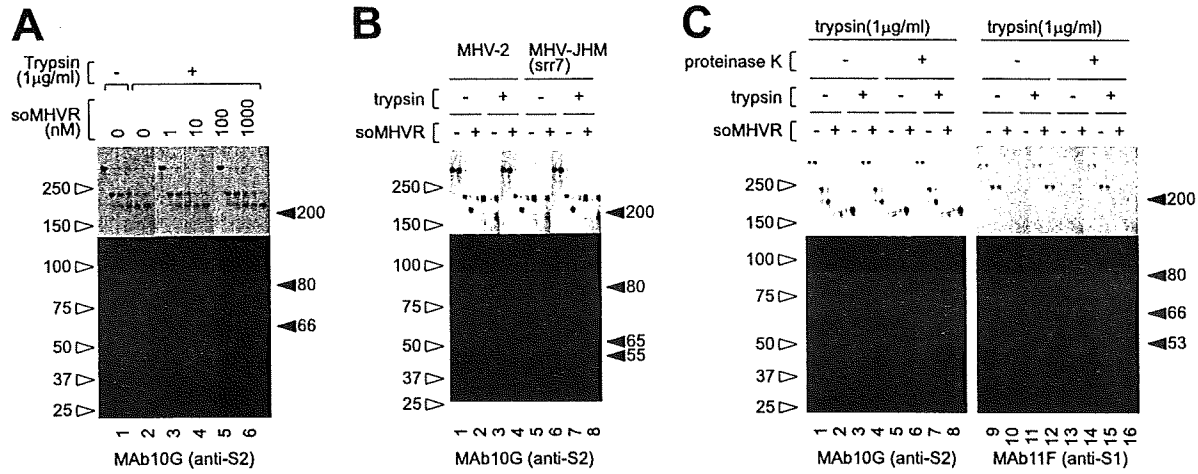

FIG. 3. Step 2 conformational change of MHV-2 S protein is induced by trypsin. (A) soMHVR concentration-dependent conformational changes induced by trypsin. Virions were incubated with various concentrations of soMHVR (lanes 3 to 6) or PBS (lanes 1 and 2), and then the samples were digested with trypsin (lanes 2 to 6). (B) Comparison of the trypsin-digested S fragment between MHV-2 and MHV-JHM-srr7. Samples were treated with 1 μM soMHVR and 1 μg of trypsin/ml as in panel A. (C) Analysis of conformational changes induced by trypsin by proteinase K digestion. Virions were incubated in the absence (lanes 2, 4, 6, 8, 10, 12, 14, and 16) or presence (lanes 1, 3, 5, 7, 9, 11, 13 and 15) of soMHVR. The samples were digested with trypsin (lanes 3, 4, 7, 8, 11, 12, 15, and 16) and then further digested with proteinase K (lanes 5 to 8 and lanes 13 to 16) and analyzed by SDS-PAGE and Western blotting with the indicated antibody.

formational changes in S that expose the fusion peptide and result in an interaction of S with the target cell membrane.

Interaction with the receptor induces changes in S that expose the trypsin recognition site. It has been well documented that trypsin treatment can activate the membrane fusion potential of MHV-2 S protein after receptor binding (18). Therefore, we next examined the fragments of S protein produced by trypsin digestion. As shown in Fig. 3A, S protein was cleaved from 200 kDa (lane 1) to 80 kDa (lane 2) by trypsin in the absence of soMHVR. However, a clear band of 66 kDa was detected when the virus was incubated with more than 1 nM soMHVR (lanes 3 to 6). The amount of 66-kDa protein increased according to the increase in concentration of added soMHVR. These results indicate that receptor binding induces the step 1 conformational changes of S protein that expose the trypsin target region and allow trypsin-mediated activation of the fusion machinery. In addition, the liposome-binding ability of MHV-2 was not enhanced by the trypsin treatment after the addition of soMHVR (data not shown). Furthermore, we compared the cleaved S proteins of srr7 to MHV2 S, as shown in Fig. 3B; an 80-kDa srr7 S2 subunit was induced by adding soMHVR (lanes 6 and 8), and 65- and 55-kDa bands became detectable after treatment of soMHVR and trypsin (lane 8) as we previously reported (12).

Both trypsin and CPL can induce six-helix bundle formation. We hypothesized that the 66-kDa form of S protein induced by soMHVR and trypsin represented the fusogenic 6HB conformation, since trypsin treatment induces cell-cell fusion in S-expressing cells. 6HB conformations are characterized by the presence of a protease-resistant core. To test this hypothesis, the 66-kDa form of S protein was further digested with proteinase K, and the proteinase K-resistant fraction was detected. As shown in Fig. 3C, a clear proteinase K-resistant 53-kDa band was detected when the virus was incubated with soMHVR and then exposed to trypsin (lane 8), but this band was greatly reduced and more disperse when the virus was incubated without soMHVR or trypsin (lanes 5 to 7). The 53-kDa protein was revealed to be a constituent of 6HB, since it was not detected when treated with HR-P (see Fig. 5, compare lane 5 with lane 6). HR-P is believed to inhibit the formation of 6HB by blocking the binding of HR-C with HR-N and consequently no apparent band corresponding to 6HB is detected after treatment with proteinase K. In contrast, the S1 subunit detected with MAb 11F was cleaved to 100 kDa by trypsin and was lost by further digestion by proteinase K (Fig. 3C, lanes 9 to 16).

It has been reported that CPL inhibitors specifically inhibit SARS-CoV S-mediated infection (22), and exogenous CPL induces cell-cell fusion in S expressing cells (3). Similarly, Qiu et al. reported the importance of CPL and cathepsin B (CPB) for infection by MHV-2 (18). Therefore, we next tested whether CPL or CPB digestion could induce the 6HB formation of the MHV-2 S protein. When MHV-2 was pretreated with soMHVR, CPL digested S protein from 200 kDa to a 71-kDa species and a slightly smaller species (Fig. 4A, lane 6), while in the absence of soMHVR CPL digestion of S protein was greatly reduced (Fig. 4A, lane 5). An 85-kDa band of S2 was also detected after treatment with trypsin or CPL in some experiments. (Fig. 5, lanes 3 and 9). To examine the molecular mass of the fragments generated by treatment with trypsin and CPL, MHV-2 was mixed with soMHVR and then digested with each protease (Fig. 4B, lanes 1 and 3). Samples treated with trypsin or CPL were mixed and loaded into a single lane of an SDS-PAGE gel to visualize any differences in mobility. As shown in Fig. 4B lane 2, the major band produced by CPL was detected at 71 kDa, a slightly larger size than the 66-kDa band produced by trypsin.

CPB also digested 200-kDa S to an 85-kDa and a 71-kDa species in the presence of soMHVR (Fig. 4A, lane 10). Combined digestion with CPB plus CPL produced bands similar to those produced by treatment with CPL alone (Fig. 4A, compare lanes 6 and 14). When the virus was further exposed to

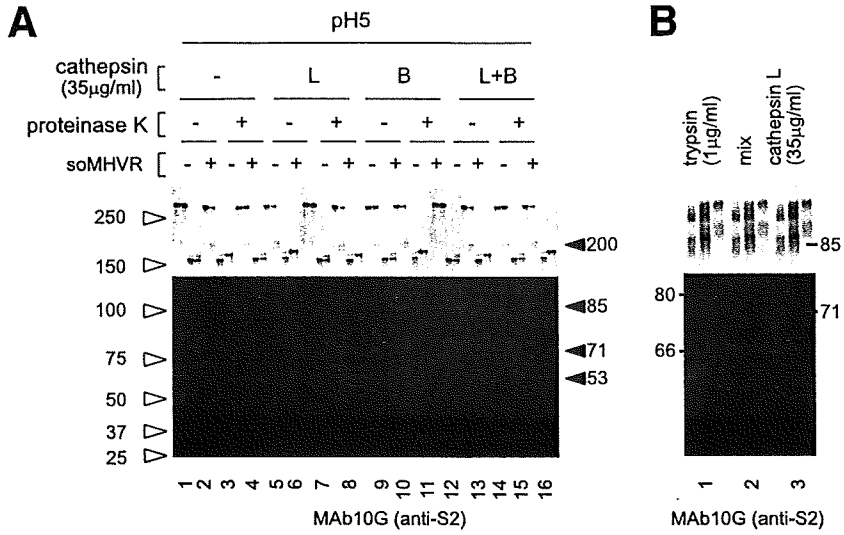

FIG. 4. Step 2 conformational change of MHV-2 S protein is induced by cathepsins. (A) Analysis of conformational changes induced by CPL or CPB. Virions incubated with soMHVR were digested with CPL (lanes 5, 6, 7, and 8), CPB (lanes 9, 10, 11, and 12), or CPL plus CPB (lanes 13, 14, 15, and 16) and digested with proteinase K (lanes 3, 4, 7, 8, 11, 12, 15, and 16). (B) Comparison of cleaved fragments between trypsin and CPL treated S protein after interaction with soMHVR. Samples digested with trypsin or CPL as shown in Fig. 3C, lane 4, and Fig. 4A, lane 6, were loaded in lanes 1 and 3, respectively. A mixture of trypsin and CPL treated S protein was loaded in lane 2.

proteinase K after incubation with soMHVR and treatment with CPL, a clear band of 53 kDa was detected, as shown in Fig. 4A, lane 8. This 53-kDa band was the same size as that produced by trypsin and proteinase K that appeared to be a component of 6HB, since this band was not detected after treatment with HRP, as shown in Fig. 5, lane 12. A 45-kDa proteinase K-resistant band was detected when MHV-2 was incubated at pH 5.0 in the presence or absence of CPL (Fig. 4A, lanes 3, 4, 7, 11, 12, and 15). This indicates that the 45-kDa form is induced by low pH, but this does not relate to fusion activity since MHV-2-infected cells fail to develop syncytia at low pH (18). These results suggest that trypsin or CPL treatment alone is sufficient to induce 6HB formation of the S protein after interaction with MHVR.

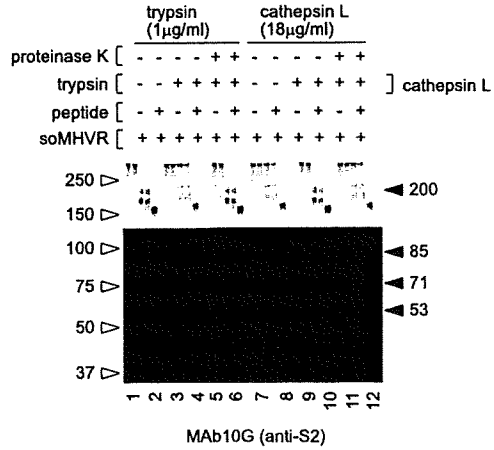

FIG. 5. S Inhibition of conformational changes by HRP. All samples were treated with soMHVR and then mixed with HRP (lanes 2, 4, 6, 8, 10, and 12) or PBS (lanes 1, 3, 5, 7, 9, and 11). The samples were treated with trypsin (lanes 3 to 6) or CPL (lanes 9 to 12) and then with proteinase K (lanes 5, 6, 11, and 12) or PBS (lanes 1 to 4 and lanes 7 to 10).

CPL induces 6HB formation but not membrane fusion. Although the 6HB formation of MHV-2 S protein could be induced by CPL cleavage, we failed to induce the direct cell-cell fusion or hemifusion of MHV-2-infected cells by CPL or CPB, detected by staining the cells with octadecyl rhodamine B (R18) and calcein blue, under the various conditions tested (data not shown). Therefore, we used a real-time PCR-based entry assay to detect fusion, which is more sensitive than the detection of syncytium formation. If CPL could trigger membrane fusion by S, MHV-2 would be able to enter cells directly from the cell surface when MHV-2 bound to its receptor was treated with CPL. As shown in Fig. 6A, 5 μg of trypsin/ml extensively facilitated the viral entry into bafilomycin-treated cells, demonstrating that trypsin activates the fusogenicity of S protein and induces fusion of the virus envelope and plasma membrane. In contrast, CPL failed to facilitate MHV-2 infection. These findings support the hypothesis that CPL treatment is not sufficient to facilitate membrane fusion.

The failure of CPL to induce viral envelope-plasma membrane fusion could be explained if CPL-treated virus is arrested at the stage of hemifusion. If this is the case, then subsequent fusion pore formation could be triggered by treatment with chlorpromazine (CPZ), a membrane-permeable cationic drug that lowers the energy requirement for forming fusion pores (15). To test the ability of CPZ to induce fusion, virus was adsorbed onto the surface of bafilomycin-treated cells, treated with CPL, and then treated with CPZ for only 3 min. As shown in Fig. 6B, virus entry was facilitated by treatment with CPZ in a concentration-dependent manner. However, virus entry into the CPZ-treated cells was only sixfold higher than in untreated cells, which is a small enhancement compared to that caused by trypsin. This weak enhancement by CPZ could be attributed to the small degree of cleavage and

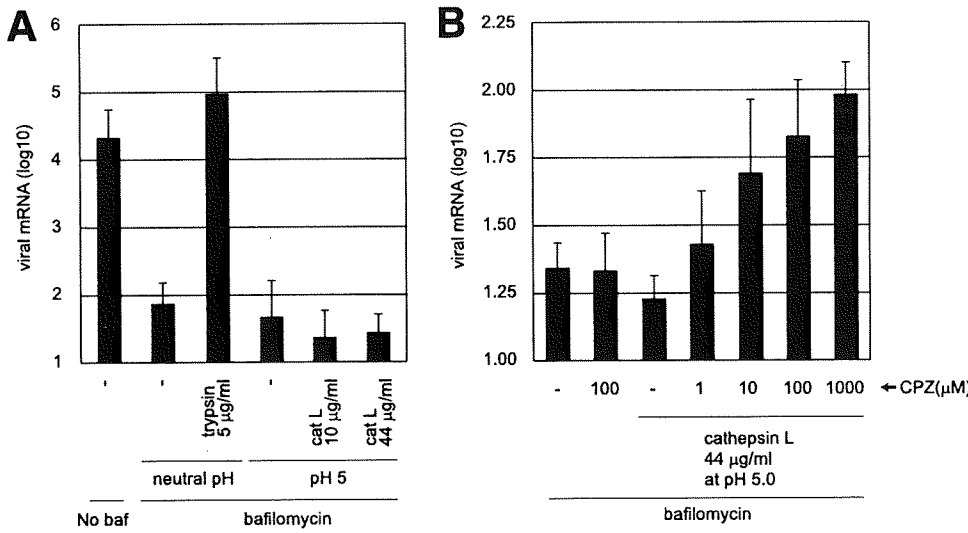

FIG. 6. Entry of MHV-2 from the cell surface is facilitated by protease and CPZ. (A) Effect of proteases on MHV-2 entry into DBT cells treated with bafilomycin. DBT cells were treated with bafilomycin for 30 min and infected with MHV-2 at a multiplicity of infection of 1. The cells were treated with trypsin or CPL and cultured in the presence of bafilomycin for a further 5 h. The amount of viral mRNA7 was measured quantitatively by real-time PCR. Cells not treated with bafilomycin or cells treated with bafilomycin but not with protease were used as controls. (B) Effect of CPZ on MHV-2 entry after treatment with CPL. DBT cells were treated with bafilomycin, infected with MHV-2, and treated with CPL as described for panel A. Immediately after CPL treatment, various concentrations of CPZ (pH 5.0) were treated for 3 min, and cells were cultured in the presence of bafilomycin for a further 5 h. The amount of viral mRNA7 was measured as described for panel A. Cells not treated with CPL or cells treated with CPZ but not with CPL were used as controls. baf, bafilomycin.

6HB formation achieved by CPL (Fig. 4A, lanes 6 and 8) compared to the more efficient cleavage by trypsin (Fig. 3C, lanes 4 and 8). The cytotoxicity of CPZ could also be responsible for the weak enhancement. Nevertheless, these results suggest that membrane fusion cannot be induced by CPL alone and that another unidentified factor that functions like CPZ must cooperate with CPL to trigger fusion of the MHV-2 envelope and the plasma membrane.

DISCUSSION

Soluble forms of receptor proteins are useful in the research of conformational changes of coronavirus S glycoproteins. However, the soluble SARS-CoV receptor (soACE2) prepared in our laboratory does not work satisfactorily for these experiments. This failure could be attributed to the previously reported insufficient neutralization activity of soACE2 compared to the clear-cut neutralization seen with soMHVR (8). Complete neutralization of pseudotyped virus bearing SARS-S was not obtained even with a high concentration of soACE2 (>200 nM), whereas 10 nM soMHVR (CEACAM1a) completely neutralized the MHV-JHM strain (16). Under these conditions, conformational changes in the S protein of SARS-CoV were not induced by soACE2 (data not shown). Proteolytic digestion by endosomal cathepsins has been described to be involved in the entry of four different enveloped viruses: ebolavirus, SARS-CoV, MHV-2, and human coronavirus 229E (5, 9, 18, 22). Cathepsins are thought to be utilized by the ebolavirus glycoprotein to generate its fusion-competent state (20), but the receptor for this virus has not been identified, and therefore a soluble form of the receptor is not available. The soluble form of aminopeptidase N, the receptor of 229E, has also not been well documented for these analyses. Therefore, the combination of MHV-2 and soMHVR is currently the only system available for the investigation of the protease-induced conformational changes in a viral glycoprotein. Our previous study using soMHVR has enabled the detection of 6HB of the MHV S protein, which is the final product of conformational changes (12). In the present study, we demonstrate the multistep conformational changes undergone by MHV-2 S protein to induce fusion. A multistep mechanism for fusion activation has also been proposed for SARS-CoV using an intervirion fusion assay (22).

Receptor-induced step 1 conformational changes. A two-step fusion activation mechanism was first reported for the avian sarcoma leukosis virus (ASLV) envelope protein, Env (17). The first step involves receptor-induced conformational changes in Env at neutral pH. The changes lead to exposure of the fusion peptide so that Env inserts its fusion peptide into the cell surface membrane. The next step involves low pH activation of Env, which results in completion of the fusion reaction in an acidic endosomal compartment, following virus uptake and endosomal trafficking. Detailed analysis of conformational changes in Env identified at least five conformational states during activation (11). Similarly, the data in our study indicate that the activation events of MHV-2 S protein can also be divided into two steps, a receptor-triggered membrane-binding step and a protease-activated step. In various viruses, such as SARS-CoV, the possibility has been reported that a prehairpin intermediate forms a stable trimer by HR-Ns (7). In the present study, we show that receptor binding induces a stable trimer that likely exists in a prehairpin conformation. This structure seems to be maintained when S protein is cut by proteases such as CPL in the endosome. Interestingly, the anti-S2A antibody bound only to the native intermediate of S

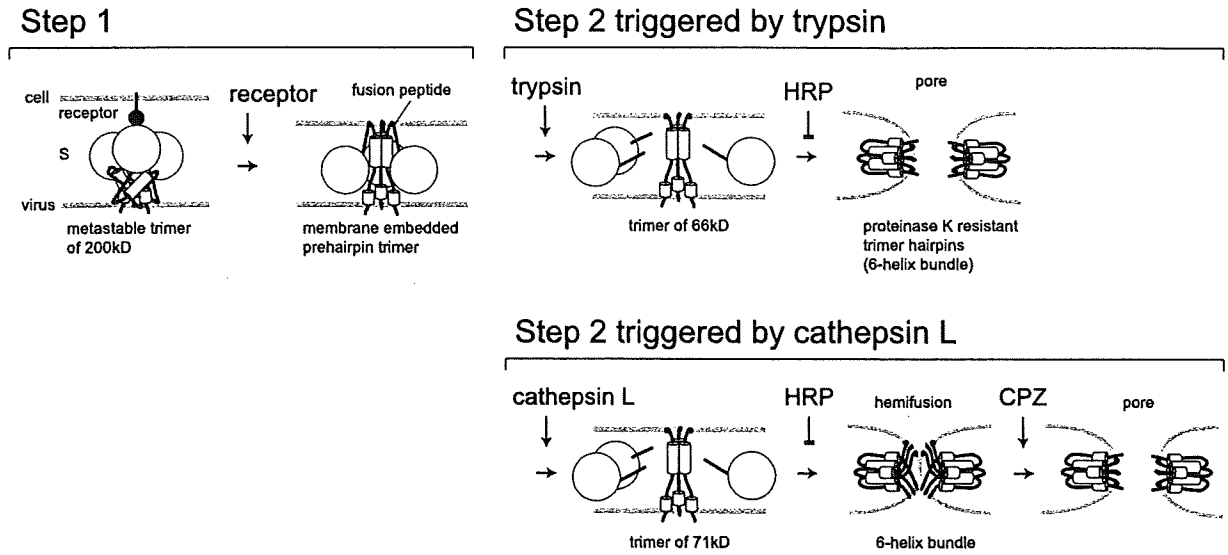

FIG. 7. Model of the two-step conformational changes of MHV-2 S protein. After receptor interaction at the cell surface, MHV-2 S protein forms a stable trimer from its metastable state, and the fusion peptide is exposed and inserted into the target membrane (step 1). Upon treatment with trypsin, the receptor-primed form of MHV-2 S protein is digested to a 65-kDa fragment, which forms a stable 6HB to make a fusion pore (step 2). However, upon treatment with CPL, S protein cannot make a fusion pore even when 6HB formation is induced. CPZ treatment facilitates pore formation of CPL-primed S protein, allowing delivery of the viral core into the cytoplasm.

that had undergone step 1 conformational changes after receptor binding. This suggests that the S2A site is exposed by receptor-induced (step 1) conformational changes out of the spike globule, which is normally not accessible to antibodies against S2A. Since the intermediate structure of S protein is not yet well studied, analysis of MHV-2 S protein with this particular antibody will aid the study of this intermediate conformation.

Protease-induced step 2 conformational changes. It was reported previously and shown in the present study that treatment of MHV-2 S protein with trypsin cleaves S2 to an 80-kDa form (18), similar to what is seen with trypsin treatment of SARS-CoV S (3). However, unlike with SARS-CoV, this cleavage event is not responsible for cell entry of MHV-2 because it occurs in the absence of receptor. In the present study, the receptor-primed form of S was cut into 66- or 71-kDa fragments of S2 by trypsin or CPL, respectively. Moreover, 66- and 71-kDa forms of S2 could form 6HB, which is thought to be the minimal size containing a fusion peptide, two HRs, and a transmembrane domain. Similarly, we and Belouzard et al. recently reported that cleavage at 120 amino acids downstream of the predicted cleavage site conferred fusion activity to the SARS-CoV S2 subunit (2, 26).

The results of our study have led to the model presented in Fig. 7, in which receptor binding and trypsin cleavage act sequentially to form distinct conformations of MHV-2 S protein that mediate virus-cell membrane fusion. Our study clearly shows that trypsin induces the complete membrane fusion of MHV-2 S protein, being consistent with SARS-CoV fusion events. However, CPL fails to induce complete membrane fusion, which is different from the observation reported for SARS-CoV S-mediated fusion (3, 22). This distinct feature of trypsin and CPL could be attributed to the small difference in the size of the residual S2 after trypsin versus CPL digestion, as revealed by detailed electrophoresis analysis (Fig. 4B). Two different groups have reported that membrane fusion is induced by CPL in SARS-CoV infection. Simmons et al. observed S protein-mediated membrane fusion by an intervirion fusion assay. Two different pseudotyped viruses were used in this assay: one with both SARS-CoV S and ASLV Env and the other expressing ACE2 and encoding luciferase. These pseudotypes were mixed, and fusion was induced by CPL; the fused pseudotypes were then allowed to infect cells expressing the ASLV receptor. Finally, infection was monitored by measuring the expression of luciferase as a result of membrane fusion between these two different pseudotype virions in vitro (22). However, ASLV can also utilize an endosomal pathway for entry. Therefore, even if the intervirion membrane fusion by S protein of SARS-CoV was not complete, i.e., arrested at the hemifusion stage, it could be completed by an unidentified factor in the endosomal environment resulting in the expression of luciferase. Bosch et al. reported significantly smaller cell-cell fusions induced in S-expressing Vero-E6 cells treated with CPL compared to the robust fusion induced by trypsin (3). However, we failed to detect SARS-CoV fusion events by CPL treatment alone, either by a cell-cell fusion assay or by the more sensitive virus-cell fusion assay used in the present study.

Our study shows that trypsin and CPL both induce similar conformational changes in S protein from a prehairpin intermediate to a folded hairpin structure. However, while membrane fusion events were completed in two steps when treated with trypsin, they were not executed in two steps when treated with CPL. The effect of trypsin could correspond to the step 2 conformational changes of ASLV Env observed in a low-pH environment. Figure 4B indicates that the CPL cleavage site is likely more N-terminal than the trypsin cleavage site. It is likely that this difference presents an obstacle to conformational

changes in S. It is possible that if the CPL-initiated 6HB formation of S protein was not complete, additional cleavage by proteinase K could contribute to the 6HB formation seen in the present study. In any case, these results show that CPL can trigger conformational changes in S protein that at least make an intermediate to achieve 6HB formation. In addition, although the S protein could form a hairpin structure after CPL treatment, it failed to induce membrane fusion. This state of S protein seems to be similar to the cold-arrested stage of ASLV Env (1). Even if the 6HB of Env is formed at a low pH, the membrane fusion event fails to proceed past hemifusion at a low temperature. Incubation at physiological temperature is critical for making a membrane pore (1).

It was reported that a mutant of influenza HA that is arrested at hemifusion can complete fusion with the aid of CPZ, a reagent that binds to the membrane and promotes formation of the fusion pore (15). In the present study, we observed that CPZ can also bring about pore formation in MHV-2-infected cells treated with CPL. However, the effect was not complete, likely due to the incomplete cleavage of S by CPL. This finding suggests that the membrane fusion event induced by CPL is arrested at a hemifusion stage, presumably because the energy of the S protein was not enough to pull and mix the membranes and another factor is necessary to stimulate S protein to overcome the energy barrier of conversion from hemifusion to complete fusion. Interestingly, it was also reported that the ebolavirus glycoprotein is activated by CPL, but it is not the final trigger to induce membrane fusion. Another, as-yet-unidentified factor is predicted to cooperate with CPL for membrane fusion (20). We speculate that another protease may cut away at the N-terminal part of the CPL fragment of S protein and allow the conversion from hemifusion to complete membrane fusion.

Alternatively, there is the possibility that endosomal membranes with a lipid composition different from that of the plasma membrane can be fused more easily with the viral envelope. A typical biological membrane is composed of hundreds of different lipids, and lipids can be delivered to a variety of organelles by selective partitioning in a series of sorting steps (14). Particularly, the cholesterol content of late endosomes and lysosomes is lower than that in the plasma membrane (21), which results in a higher flexibility of membranes in these organelles. In addition, many kinds of viral receptors on the plasma membrane are reported to localize to lipid rafts, which contain a heavy concentration of cholesterol and thus are not very flexible. Since virus carried into late endosomes encounters a more flexible membrane, virus-cell membrane fusion could be induced with lower energy. Another possibility is that clathrin depletion enhances the membrane fusion on the cell surface, since CPZ is also known as an inhibitor of clathrin-coated pit formation at the cell surface. Reduction of the netlike structure made of clathrin would result in a more flexible surface. Thus, it may be possible that CPL is able to induce virus-cell membrane fusion in the endosome but not on the plasma membrane, whereas trypsin can successfully induce cell-cell and virus-cell membrane fusion on the plasma membrane. Studies are in progress to examine this possibility using liposomes with different lipid compositions.

ACKNOWLEDGMENTS

We thank B. J. Bosch and P. J. Rottier (Utrecht University) for providing the heptad repeat peptide and K. L. Schornberg, D. Dube, S. E. Delos, and J. M. White (University of Virginia) for valuable comments on this work.

This study was supported by a Ministry of Education, Culture, Sports, Science, and Technology grant and by grants from the Uehara Memorial Foundation and the Ichiro Kanehara Foundation.

REFERENCES

1. **Barnard, R. J. O., D. Elleder, and J. A. T. Young.** 2006. Avian sarcoma and leukosis virus-receptor interactions: from classical genetics to novel insights into virus-cell membrane fusion. Virology **344**:25–29.
2. **Belouzard, S., V. C. Chu, and G. R. Whittaker.** 2009. Activation of the SARS coronavirus spike protein via sequential proteolytic cleavage at two distinct sites. Proc. Natl. Acad. Sci. USA **106**:5871–5876.
3. **Bosch, B. J., W. Bartelink, and P. J. M. Rottier.** 2008. Cathepsin L functionally cleaves the severe acute respiratory syndrome coronavirus class I fusion protein upstream of rather than adjacent to the fusion peptide. J. Virol. **82**:8887–8890.
4. **Bosch, B. J., R. van der Zee, C. A. M. de Haan, and P. J. M. Rottier.** 2003. The coronavirus spike protein is a class I virus fusion protein: structural and functional characterization of the fusion core complex. J. Virol. **77**:8801–8811.
5. **Chandran, K., N. J. Sullivan, U. Felbor, S. P. Whelan, and J. M. Cunningham.** 2005. Endosomal proteolysis of the Ebola virus glycoprotein is necessary for infection. Science **308**:1643–1645.
6. **Damico, R. L., J. Crane, and P. Bates.** 1998. Receptor-triggered membrane association of a model retroviral glycoprotein. Proc. Natl. Acad. Sci. USA **95**:2580–2585.
7. **Deng, Y., J. Liu, Q. Zheng, W. Yong, and M. Lu.** 2006. Structures and polymorphic interactions of two heptad-repeat regions of the SARS virus S2 protein. Structure **14**:889–899.
8. **Fukushi, S., T. Mizutani, M. Saijo, S. Matsuyama, N. Miyajima, F. Taguchi, S. Itamura, I. Kurane, and S. Morikawa.** 2005. Vesicular stomatitis virus pseudotyped with severe acute respiratory syndrome coronavirus spike protein. J. Gen. Virol. **86**:2269–2274.
9. **Kawase, M., K. Shirato, S. Matsuyama, and F. Taguchi.** 2008. Protease-mediated entry via the endosome of human coronavirus 229E. J. Virol. **83**:712–721.
10. **Lewicki, D. N., and T. M. Gallagher.** 2002. Quaternary structure of coronavirus spikes in complex with carcinoembryonic antigen-related cell adhesion molecule cellular receptors. J. Biol. Chem. **277**:19727–19734.
11. **Matsuyama, S., S. E. Delos, and J. M. White.** 2004. Sequential roles of receptor binding and low pH in forming prehairpin and hairpin conformations of a retroviral envelope glycoprotein. J. Virol. **78**:8201–8209.
12. **Matsuyama, S., and F. Taguchi.** 2002. Receptor-induced conformational changes of murine coronavirus spike protein. J. Virol. **76**:11819–11826.
13. **Matsuyama, S., M. Ujike, S. Morikawa, M. Tashiro, and F. Taguchi.** 2005. Protease-mediated enhancement of severe acute respiratory syndrome coronavirus infection. Proc. Natl. Acad. Sci. USA **102**:12543–12547.
14. **Maxfield, F. R., and T. E. McGraw.** 2004. Endocytic recycling. Nat. Rev. Mol. Cell Biol. **5**:121–132.
15. **Melikyan, G. B., S. Lin, M. G. Roth, and F. S. Cohen.** 1999. Amino acid sequence requirements of the transmembrane and cytoplasmic domains of influenza virus hemagglutinin for viable membrane fusion. Mol. Biol. Cell **10**:1821–1836.
16. **Miura, H. S., K. Nakagaki, and F. Taguchi.** 2004. N-terminal domain of the murine coronavirus receptor CEACAM1 is responsible for fusogenic activation and conformational changes of the spike protein. J. Virol. **78**:216–223.
17. **Mothes, W., A. L. Boerger, S. Narayan, J. M. Cunningham, and J. A. Young.** 2000. Retroviral entry mediated by receptor priming and low pH triggering of an envelope glycoprotein. Cell **103**:679–689.
18. **Qiu, Z., S. T. Hingley, G. Simmons, C. Yu, J. Das Sarma, P. Bates, and S. R. Weiss.** 2006. Endosomal proteolysis by cathepsins is necessary for murine coronavirus mouse hepatitis virus type 2 spike-mediated entry. J. Virol. **80**:5768–5776.
19. **Routledge, E., R. Stauber, M. Pfleiderer, and S. G. Siddell.** 1991. Analysis of murine coronavirus surface glycoprotein functions by using monoclonal antibodies. J. Virol. **65**:254–262.
20. **Schornberg, K., S. Matsuyama, K. Kabsch, S. Delos, A. Bouton, and J. White.** 2006. Role of endosomal cathepsins in entry mediated by the Ebola virus glycoprotein. J. Virol. **80**:4174–4178.
21. **Schulze, H., T. Kolter, and K. Sandhoff.** 2008. Principles of lysosomal membrane degradation: cellular topology and biochemistry of lysosomal lipid degradation. Biochim. Biophys. Acta **1793**:674–683.
22. **Simmons, G., D. N. Gosalia, A. J. Rennekamp, J. D. Reeves, S. L. Diamond, and P. Bates.** 2005. Inhibitors of cathepsin L prevent severe acute

respiratory syndrome coronavirus entry. Proc. Natl. Acad. Sci. USA **102:** 11876–11881.

23. **Simmons, G., J. D. Reeves, A. J. Rennekamp, S. M. Amberg, A. J. Piefer, and P. Bates.** 2004. Characterization of severe acute respiratory syndrome-associated coronavirus (SARS-CoV) spike glycoprotein-mediated viral entry. Proc. Natl. Acad. Sci. USA **101:**4240–4245.
24. **Song, H. C., M.-Y. Seo, K. Stadler, B. J. Yoo, Q.-L. Choo, S. R. Coates, Y. Uematsu, T. Harada, C. E. Greer, J. M. Polo, P. Pileri, M. Eickmann, R. Rappuoli, S. Abrignani, M. Houghton, and J. H. Han.** 2004. Synthesis and characterization of a native, oligomeric form of recombinant severe acute respiratory syndrome coronavirus spike glycoprotein. J. Virol. **78:**10328–10335.
25. **Taguchi, F., and Y. K. Shimazaki.** 2000. Functional analysis of an epitope in the S2 subunit of the murine coronavirus spike protein: involvement in fusion activity. J. Gen. Virol. **81:**2867–2871.
26. **Watanabe, R., S. Matsuyama, K. Shirato, M. Maejima, S. Fukushi, S. Morikawa, and F. Taguchi.** 2008. Entry from the cell surface of severe acute respiratory syndrome coronavirus with cleaved S protein as revealed by pseudotype virus bearing cleaved S protein. J. Virol. **82:**11985–11991.
27. **White, J. M., S. E. Delos, M. Brecher, and K. Schornberg.** 2008. Structures and mechanisms of viral membrane fusion proteins: multiple variations on a common theme. Crit. Rev. Biochem. Mol. Biol. **43:**189–219.
28. **Zelus, B. D., J. H. Schickli, D. M. Blau, S. R. Weiss, and K. V. Holmes.** 2003. Conformational changes in the spike glycoprotein of murine coronavirus are induced at 37°C either by soluble murine CEACAM1 receptors or by pH 8. J. Virol. **77:**830–840.

Microbiol Immunol 2009; **53**: 75–82
doi:10.1111/j.1348-0421.2008.00097.x

ORIGINAL ARTICLE

Neutralizing antibody against severe acute respiratory syndrome (SARS)-coronavirus spike is highly effective for the protection of mice in the murine SARS model

Koji Ishii[1], Hideki Hasegawa[2], Noriyo Nagata[2], Yasushi Ami[3], Shuetsu Fukushi[4], Fumihiro Taguchi[5] and Yasuko Tsunetsugu-Yokota[6]

[4]Department of Virology I, [1]Department of Virology II, [5]Department of Virology III, [2]Department of Pathology, [3]Division of Experimental Animals Research and [6]Department of Immunology, National Institute of Infectious Diseases, Toyama, Shinjuku-ku, Tokyo 162-8640, Japan

ABSTRACT

We evaluated the efficacy of three SARS vaccine candidates in a murine SARS model utilizing low-virulence Pp and SARS-CoV coinfection. Vaccinated mice were protected from severe respiratory disease in parallel with a low virus titer in the lungs and a high neutralizing antibody titer in the plasma. Importantly, the administration of spike protein-specific neutralizing monoclonal antibody protected mice from the disease, indicating that the neutralization is sufficient for protection. Moreover, a high level of IL-6 and MCP-1 production, but not other 18 cytokines tested, on days 2 and 3 after SARS-CoV infection was closely linked to the virus replication and disease severity, suggesting the importance of these cytokines in the lung pathogenicity of SARS-CoV infection.

Key words coronavirus, *Pasteurella pneumotropica*, severe acute respiratory syndrome (SARS).

A new disease called SARS originated in China in late 2002 and spread rapidly throughout a number of countries. Structural characterization of the SARS-CoV and characterization of its complete RNA genome (1–3) have provided us with the opportunity to develop a SARS vaccine. Like other coronaviruses, SARS-CoV is a plus-stranded RNA virus with a 30-kb genome encoding replicase gene products and four structural proteins (i.e. spike [S], envelope [E], membrane [M], and nucleocapsid [N]) (1, 2). The S protein is a type I fusion protein with an approximate molecular weight of 180 kDa. The angiotensin-converting enzyme 2 (ACE2) has been reported to function as a receptor for SARS-CoV (4), and amino acids 270–510 of the S protein are required for interaction with the receptor (5), suggesting that the S protein would be an ideal target for a vaccine. In fact, passive transfer of neutralizing antibody can prevent replication of the SARS-CoV in the mouse respiratory tract (6, 7), and many vaccine studies of SARS-CoV have identified the S protein among other SARS-CoV structural proteins as a major determinant of neutralization (8).

Developing an animal model is crucial for evaluating the vaccine efficacy on SARS-CoV-induced lung pathogeneses. SARS-CoV infection occurs transiently in the mouse and the virus is cleared by day 7 postinfection (7), although an age-related susceptibility to lung disease in old mice has been shown (9). In the course of studying the cell entry mechanism of SARS-CoV, we found that some proteases, such as trypsin and elastase, produced in the host animals enhance SARS-CoV infection in cultured cells (10). In a previous study, we examined whether weak inflammation in the lungs induced by low-pathogenicity bacterial infection, which could induce elastase, enhances SARS-CoV infection and we showed that low-virulence

Correspondence
Yasuko Tsunetsugu-Yokota, Department of Immunology, National Institute of Infectious Diseases, Shinjuku-ku, Tokyo 162-8640, Japan. Tel: +81 3 5285 1111 ext. 2133; fax: +81 3 5285 1150; email: yyokota@nih.go.jp

Received 2 September 2008; revised 5 October 2008; accepted 22 October 2008

List of Abbreviations: CoV, coronavirus; IFN, interferon; Ig, immunoglobulin; IL, interleukin; IP, IFN-inducible protein; MCP, monocyte-chemotactic protein; Pp, *Pasteurella pneumotropica*; SARS, severe acute respiratory syndrome; s.c., subcutaneously; TNF, tumor necrosis factor.

Pp infection, as well as administration of lipopolysaccharide derived from *Escherichia coli*, induced elastase in the lungs and enhanced the replication of SARS-CoV, which resulted in the exacerbated respiratory disease caused by SARS-CoV infection with a high mortality rate. These results indicate that coinfection of SARS-CoV with low-virulence microorganisms induces exacerbated pneumonia and suggest the possibility that elastase is involved in the pathogenesis of exacerbated pneumonia caused by SARS-CoV infection (11).

In our research group, UV-inactivated and UV- and formalin-inactivated whole virion vaccines were produced and both were shown to be effective on the elicitation of persistent neutralizing antibodies accompanied by T-cell responses (12). We also constructed a replication-deficient recombinant vaccinia virus, DIs, expressing one or more SARS-CoV structural proteins (E, M, N and S, or a combination of E, M and S (E/M/S) or E, M, N and S (E/M/N/S)) (13). When these recombinant DIs vaccines were given to mice either s.c. or intranasally, the humoral and cellular immunities against SARS-CoV were elicited. We showed that a high level of serum neutralizing IgG antibody elicited by subcutaneous injection of these vaccinias strongly suppressed SARS-CoV replication in the lungs and that the neutralizing IgA-type antibody elicited only by mucosal (intranasal) immunization was not absolutely required. Furthermore, we demonstrated that DIs expressing the S protein alone or in combination with other components, but not N alone, elicited strong neutralizing antibody and T-cell responses against SARS-CoV infection. Although we and others demonstrated that the vaccine expressing the S protein alone was able to inhibit SARS-CoV replication efficiently in mice, the role of the N-specific T-cell response for protection had not been formally excluded, because the SARS-CoV infection in mice is usually cleared rapidly without causing any pulmonary disease.

Utilizing a murine model system of severe respiratory disease caused by the coinfection of Pp and SARS-CoV, we here evaluated the protective efficacy of our SARS vaccine candidates: UV- or UV-plus-formalin-inactivated whole virion and recombinant DIs expressing the S protein only. We have monitored the bodyweight and analyzed the virus replication and cytokine production in the lung lavage of vaccinated and naïve mice after SARS-CoV infection. By giving SKOT-20 monoclonal neutralizing antibody recognizing the S protein just before Pp infection, the mortality of mice coinfected with Pp and SARS-CoV was dramatically reduced in a dose-dependent manner. These results clearly show that the neutralizing antibody against S protein is highly effective and sufficient to prevent SARS development. Furthermore, we found that IL-6 and MCP-1 production was associated with high titers of SARS-CoV, suggesting the possible link between the increased production of these cytokines and the lung pathogenicity caused by Pp and SARS-CoV coinfection.

MATERIALS AND METHODS

Virus and virus titration

Fr-mo, the mouse-adapted Frankfurt-1 (Fr-1) strain created by passaging 10 times through the mice and finally grown in VeroE6 cells, was propagated and plaque assayed with VeroE6 cells as previously described (10). VeroE6 cells were grown and maintained in Dulbecco's modified minimal essential medium (DMEM; Nissui, Tokyo, Japan) and virus infectivity was determined by plaque assay as previously described (10).

Preparation of UV- or UV-and-formalin-inactivated purified SARS-CoV

UV-inactivated purified SARS-CoV (UV-V) was prepared as previously described (14). In brief, SARS-CoV (HKU29849) was amplified in Vero E6 cells, exposed to UV light (4.75 J/cm^2), and then purified by sucrose density gradient centrifugation. A portion of the UV-inactivated purified virions was further treated overnight with 0.02% formalin (UV-F-V) to assure the safety of a whole virion vaccine (12).

Vaccination

Animal studies were carried out under a protocol approved by the Animal Care and Use Committee of the National Institute of Infectious Diseases, Japan. Six-week-old BALB/c male mice were purchased from SLC(Hamamatsu, Japan) or Charles River Japan (CRJ, Tokyo, Japan). These mice are serologically checked to be free from infections with pathogenic microorganisms, including Pp. For vaccination with recombinant DIs, mice were s.c. immunized with 10^6 plaque-forming units (p.f.u.) of rDIs-SARS-S or DIs (as a negative control). After 4 weeks, identical titers of viruses were re-administered. For vaccination with a whole inactivated virion, mice were s.c. injected into the back with 10 μg UV-V or UV-F-V with 2 mg alum, and boosted by the same procedure 7 weeks after priming. One week later, mice were anesthetized with xylazine and ketamine by intraperitoneal (i.p.) administration and intranasally inoculated with 6×10^6 colony-forming units (c.f.u.) of Pp MaM strain (11) suspended in 20 μL PBS and kept in globe box isolators in a BSL 3 laboratory in our institute during the experimental period. One day later, the mice were intranasally challenged with 0.8×10^6 $TCID_{50}$ of SARS-CoV in 20 μL saline as previously described (11). Three, 5, and 7 days after challenge by SARS-CoV, serum,

nasal and lung lavage fluids were collected to measure viral titers and antibodies against SARS-CoV from mice that were killed under anesthesia with chloroform. The bodyweight of these mice was measured every day.

Detection of SARS-CoV-specific antibodies

IgG titers against SARS-CoV were determined by ELISA as previously described (14). Neutralization antibody titers were determined as previously described (15). Briefly, samples were heat-inactivated and diluted twofold from 1:80 to 1:5120 with DMEM containing 5% fetal bovine serum and 3000 infectious units of vesicular stomatitis virus (VSV) pseudotype-bearing SARS-CoV S protein (VSV-SARS-St19). The mixture was incubated for 1 hr at 37 °C for neutralization. After incubation, the mixture was inoculated onto Vero E6 cells seeded on 96-well plates. The infectivity of VSV-SARS-St19 was determined by counting the number of green fluorescence protein (GFP)-positive cells. The Nab titer was defined as the reciprocal of the highest dilution at which more than 50% inhibition of infectivity was observed.

Analysis of cytokines and chemokines

Cytokines and chemokines were assayed either using a mouse inflammatory cytokine (IL-6, IL-10, MCP-1, IFN-γ, TNF-α and IL-12p70) cytometric bead array kit (Becton Dickinson, San Jose, CA, USA) (12) or using the Luminex 200 system (Luminex Co., Austin, TX, USA) as previously reported (16). Lung homogenates prepared as described above were diluted 1:10 with a lysis buffer and viruses included in the materials were completely inactivated by UV irradiation for 10 min. In the Luminex system, the following cytokines and chemokines were measured by a mouse cytokine 20 plex antibody bead kit (Bioscience International, Inc., Camarillo, CA, USA): fibroblast growth factor basic, granulocyte–macrophage colony-stimulating factor, IFN-γ, IL-10, IL-12, IL-13, IL-17, IL-1α, IL-1β, IL-2, IL-4, IL-5, IL-6, IL-10, keratinocyte-derived chemokine (KC), MCP-1, monokine-induced by IFN-γ, IFN-inducible protein (IP)-10, TNF-α, and vascular endothelial growth factor (VEGF).

RESULTS

Efficacy of a whole inactivated SARS-CoV virion vaccine and recombinant DIs expressing S protein

We studied the SARS vaccine efficacy using a recently established murine SARS model (11). In this model, a low-virulence Pp infection exacerbates lung pathogenesis associated with SARS-CoV infection.

We first examined the protective efficacy of UV- and UV-plus-formalin-inactivated whole virion (UV-V and UV-F-V, respectively). Twelve mice in each group were s.c. inoculated with 10 μg UV-V or UV-F-V with alum, or alum in PBS (alum only) as a control, booster immunized with the same vaccines at 7 weeks, and then infected with Pp intranasally 1 week later. One day after the infection of Pp, mice were intranasally infected with a mouse-adapted strain of SARS-CoV (Fr-mo). Although Pp is of low virulence and causes only a mild respiratory disease, Pp-infected mice showed a transient loss of bodyweight and ruffled hair from 1 to 3 days postinfection and then gradually recovered. However, mice coinfected with SARS-CoV 1 day after Pp infection had severe weight loss and showed high mortality with exacerbated pneumonia (11). In this murine model of SARS, both control and UV-V- or UV-F-V-vaccinated mice showed a transient decrease in bodyweight until day 2 after SARS-CoV infection (Fig. 1). Then, most of the vaccinated mice recovered to their original weight before SARS-CoV infection, whereas control mice (alum only) continuously lost weight and 90% died at day 7 postinfection.

In a second set of experiments, mice were immunized with recombinant DIs-S or empty DIs (as a negative control: DIs-cont) 5 weeks and 1 week before Pp infection, and infected with SARS-CoV the next day. Similar to the results of whole virion vaccines as described above, mice vaccinated with DIs showed transient and minimal clinical symptoms, such as ruffled hair and weight loss until 3 days after Fr-mo infection (Fig. 2, left). Severe symptoms continued during the observation period in control mice. On days 4–7 after virus infection, these mice suffered the loss of 40% or more of their bodyweight, and more than 80% of those mice died after exhibiting severe respiratory disease, whereas none of the mice vaccinated with recombinant DIs expressing S proteins died (Fig. 2, right). To further evaluate the vaccine effect, we measured serum neutralizing antibody and SARS-CoV titer in the lung lavage of vaccinated mice. Before Pp and SARS-CoV coinfection, vaccinated mice developed a high level of anti-SARS-CoV IgG with neutralizing activity (data not shown). As shown in Figure 3a, a high level of neutralizing antibody was maintained during coinfection experiments, at day 3 until day 7 postinfection in all vaccinated mouse groups. The SARS-CoV titer in the lung lavage was high at day 3 postinfection, decreased at day 5 (Fig. 3b, blank column: alum only and DIs-cont) and virus became undetectable at day 7 (data not shown). In contrast, the virus titers were significantly reduced in parallel with a high titer of plasma neutralizing antibody in all vaccinated groups (Fig. 3a). Therefore, both whole virion vaccines and vaccinia vector expressing spike protein were protective from a highly pathogenic pulmonary infection of SARS-CoV in

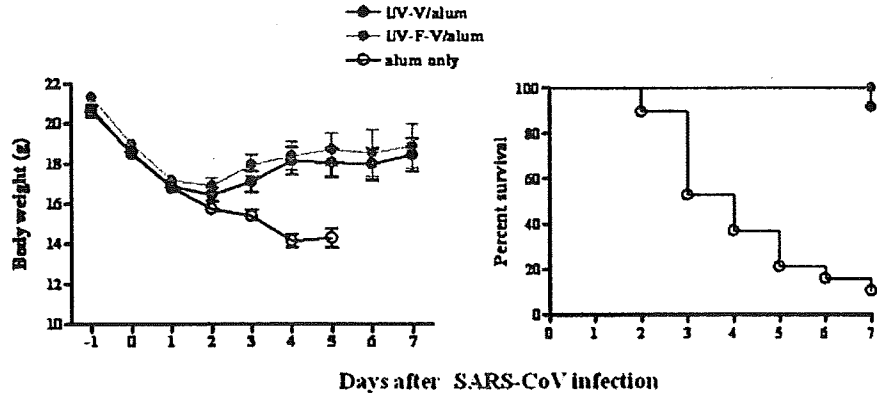

Fig. 1. (Left) Bodyweights of mice vaccinated with inactivated virions in a murine model system of severe respiratory disease caused by the coinfection of Pp and SARS-CoV. Mice were s.c. injected on the back with 10 μg UV-V or UV-F-V with 2 mg alum, and boosted by the same procedure 7 weeks after priming. One week later, mice were infected intranasally with Pp (6×10^6 c.f.u. day -1) and 1 day later with SARS-CoV (0.8×10^6 p.f.u. Fr-mo, day 0), and were weighed daily after Pp infection. Mice were vaccinated with UV-inactivated virions with alum (●), UV- and-formalin-inactivated virions with alum (○), or alum only (○). The number of mice used in this study was 17 (UV-V), 12 (UV-F-V) and 17 (alum), respectively. Bar shows the standard error of the mean (SEM). (Right) Survival curves of mice vaccinated with inactivated virions.

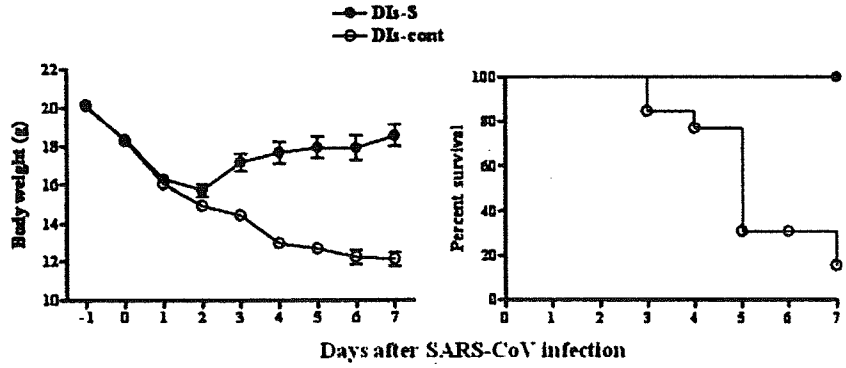

Fig. 2. (Left) Bodyweights of mice vaccinated with recombinant DIs in a murine model system of severe respiratory disease caused by the coinfection of Pp and SARS-CoV. Mice were i.p. injected with 10^6 p.f.u. of rDIs-SARS-S or DIs, and boosted by the same procedure 4 weeks after priming. One week later, mice were infected intranasally with Pp (day -1) and 1 day later with SARS-CoV (day 0), and were weighed daily after Pp infection. Mice were vaccinated with rDIs-SARS-S (●) or DIs only (○). Bar shows the SEM ($n = 18$). (Right) Survival curves of mice vaccinated with recombinant vaccinia virus.

the presence of opportunistic infection by Pp in this case. Furthermore, the results by DIs-S vaccine suggest that the neutralizing antibody against SARS-CoV spike protein alone is highly effective for the prevention of SARS development.

Inflammatory cytokines are suppressed in vaccinated mice

Ami *et al.* (11) demonstrated previously that the levels of IP-10 and IFN-γ are significantly high in SARS-CoV-infected and Pp/SARS-CoV-coinfected mouse lung homogenates at 2 days after SARS-CoV infection. However, these cytokines became undetectable at day 4 postinfection. To better understand the involvement of cytokines in the lung pathogenesis of SARS, we simultaneously measured six cytokines (IL-6, IL-10, MCP-1, IFN-γ, TNF-α and IL-12p70) in the lung lavage of vaccinated or unvaccinated mice at day 3 after SARS-CoV infection, when viruses replicate most extensively and vaccinated mice experienced maximum weight loss. As shown in Figure 4, the increased production of MCP-1 and IL-6 in the lungs of the control mouse group (alum and DIs-cont) was strongly suppressed in vaccinated mice, which were able to control virus replication. Increased production of other cytokines, including TNF-α, was not observed. Therefore, it is possible that IL-6 and MCP-1 play a role in the establishment of lung pathology in the Pp and SARS-CoV coinfection model.

Neutralizing monoclonal antibody against S protein is highly effective for protection

It is known that many of the neutralizing antibodies against SARS-CoV recognize a receptor-binding domain (RBD) in S1 of the spike protein, although other N-terminal domains of the S1 and S2 domains also have neutralizing epitopes (8). Previously, we established four S-protein-specific monoclonal antibodies with potent *in vitro* neutralization activity (17). Among them, a major

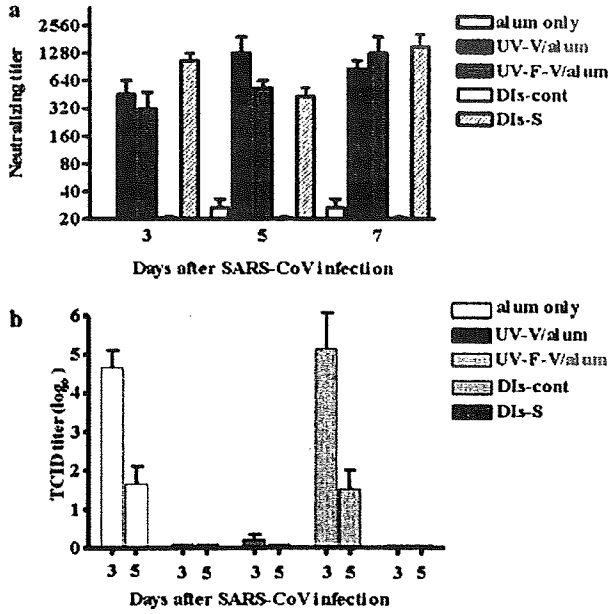

Fig. 3. (a) Neutralizing titers in the plasma of vaccinated mice. Titers were calculated as previously described (15). (b) SARS-CoV titers in the lung lavage of vaccinated mice. Bar shows the SEM ($n = 3$).

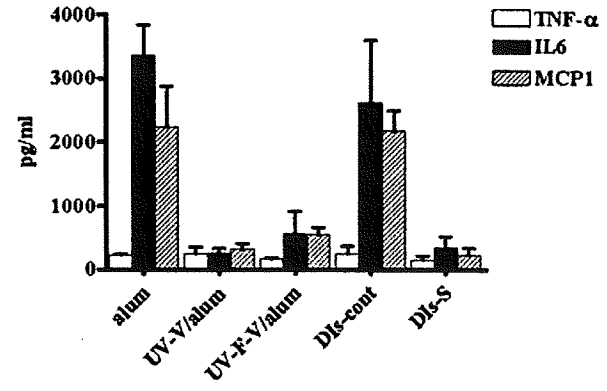

Fig. 4. Concentrations of TNF-α, IL-6 and MCP-1 in the lung lavage of vaccinated mice. Cytokines and chemokines in the lung lavage of vaccinated and control mice on day 3 after SARS-CoV infection were assayed by flow cytometry using a mouse inflammatory cytokine (IL-6, IL-10, MCP-1, IFN-γ, TNF-α and IL-12p70) cytometric bead array kit. Bar shows the SEM ($n = 3$).

epitope of SKOT-20 localizes to the RBD of the S protein and exhibits the most potent neutralizing activity (18). To demonstrate that the anti-spike neutralizing antibody is mainly responsible for the protective efficacy we observed in SARS model mice, we administered SKOT-20 i.p. once, just before Pp infection. As shown in Figure 5a, the mice treated with SKOT-20 recovered from the loss of bodyweight and were resistant to the fatal outcome as we observed in vaccinated mice.

When we measured a virus titer in the lung lavage at day 3 after SARS-CoV infection, it was dramatically decreased in accordance with the concentration of neutralizing antibody given (Fig. 5b). The level of serum neutralizing antibody in these mice was proportionally high at this time point. The neutralizing activity was low but still detectable in the lung lavage. These results clearly show that the neutralizing antibody against S protein is highly effective to prevent SARS development.

Kinetics of cytokine and chemokine production

We have observed a high level of IL-6 and MCP-1 production in Pp and SARS-CoV-coinfected mouse lung lavage at day 3 after SARS-CoV infection (Fig. 4). However, the cytokine profiles in these mice may be variably modified by Pp infection alone, SARS-CoV infection, or both. Therefore, we measured 20 cytokines in lung lavages of these protected and unprotected mice by using a mouse cytokine 20-plex antibody bead kit at day 0 (after Pp infection before SARS-CoV infection), day 1, day 2 and day 3 after SARS-CoV infection as previously reported (16). The production of two cytokines, IL-6 and MCP-1, were increased at days 2 and 3 after SARS-CoV infection in association with high titers of SARS-CoV, as shown in Figure 4. Interestingly, the production of IL-6 was increased by Pp infection alone, decreasing on day 1 and increasing again, whereas that of MCP-1 increased only after SARS-CoV infection. These cytokines were not increased in protected mice (Fig. 6a), suggesting the importance of these two cytokines in the lung pathogenesis. Other cytokine profiles are shown in Figure 6b and c. The level of IP-10 was quite high after SARS-CoV infection on day 1. However, even protected mice produced a high level of IP-10. In contrast, macrophage inflammatory protein (MIP)-1α, TNF-α, and KC were produced only before SARS-CoV infection and the levels of IFN-γ and VEGF were consistently low. The concentrations of other cytokines were low or below the limit of detection (data not shown). These results suggest that IL-6 and MCP-1 play some roles in the lung pathogenicity by Pp and SARS-CoV coinfection.

DISCUSSION

In the present study, we evaluated the protective efficacy of our SARS vaccine candidates: UV- or UV-plus-formalin-inactivated whole virion and recombinant DIs expressing the S protein (DIs-S) using a murine model system of severe respiratory disease caused by the coinfection of Pp and SARS-CoV. The results shown in this paper suggest that whole virion vaccines, either with or without formalin treatment, and DIs-S were protective against a

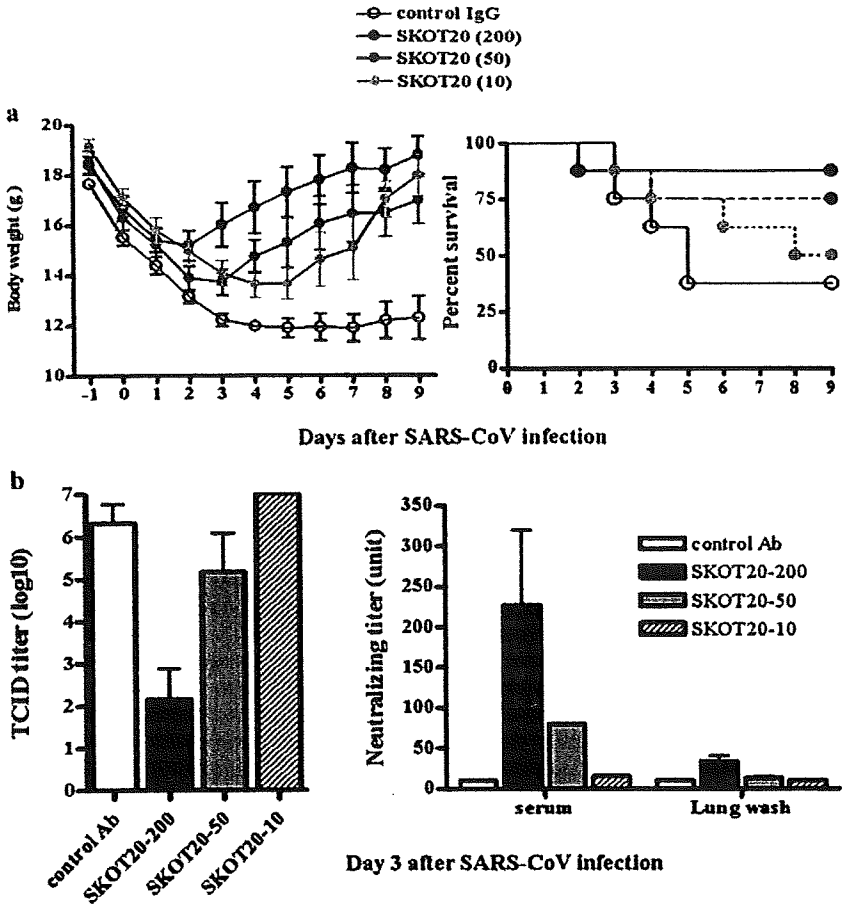

Fig. 5. (a) (Left) Bodyweights of mice injected with SKOT-20 in a murine model system of severe respiratory disease caused by the coinfection of Pp and SARS-CoV. Mice were i.p. injected with 10, 50 or 200 μg SCOT-20 just before Pp infection and weighed daily. Mice were injected with 10 μg (⊛), 50 μg (◉), or 200 μg (●) of SKOT-20 or 200 μg control IgG (○). Bar shows the SEM ($n > 8$). (Right) Survival curves of mice injected with SKOT-20. (b) (Left) SARS-CoV titers in the lung lavage of mice injected with SKOT-20. (Right) Neutralizing titers in serum and lung lavage of mice injected with SKOT-20. Bar shows the SEM ($n = 3$).

highly pathogenic pulmonary infection of SARS-CoV in the presence of opportunistic infection by Pp. By giving SKOT-20 just before SARS-CoV infection, the mortality of mice coinfected with Pp and SARS-CoV was dramatically reduced. The level of serum neutralizing antibody in these mice was proportionally high and a virus titer in the lung lavage after SARS-CoV infection was substantially decreased in accordance with the concentration of neutralizing antibody given. Therefore, if a high titer of neutralizing IgG antibody against the S protein is systemically elicited by vaccination, it would be sufficient to prevent SARS development.

Treatment with convalescent plasma has been successfully used to treat SARS, suggesting that passive immunity might be a useful approach by which to combat SARS. (19) Subbarao *et al.* have shown that passive transfer of murine neutralizing antibodies can prevent replication of SARS-CoV in the respiratory tract (20). This antibody has been shown to neutralize the virus *in vitro* and to prevent viral replication in a mouse model of SARS-CoV infection. Sui *et al.* have investigated the antiviral activity of a human monoclonal antibody to the S1 protein that blocks receptor association (21), demonstrating the prophylactic effectiveness of this monoclonal antibody *in vivo* using a mouse model of SARS (9). Recently, several humanized monoclonal antibodies against the S protein have been developed for therapeutic application (22, 23). Many of the neutralizing antibodies against SARS-CoV recognize a RBD in S1 of the spike protein, but other N-terminal domains of the S1 and S2 domains also have neutralizing epitopes (8). For the passive immunization to be highly effective, a combination of neutralizing antibodies recognizing several epitopes of the S protein should be designed so that virus escape mutation can be prevented.

The involvement of cytokines in the SARS pathogenesis has been described (24–26). When the levels of various cytokines and chemokines in the lungs of mice infected with Pp and SARS-CoV were measured, high levels of only IP-10 and IFN-γ production were noted on day 2 following coinfection, but not on day 4 (11). Therefore, the involvement of these cytokines in the high pathogenesis caused by a coinfection with Pp and SARS CoV has been suggested. In this study, we observed that the production of IL-6 and MCP-1 were increased at day 3

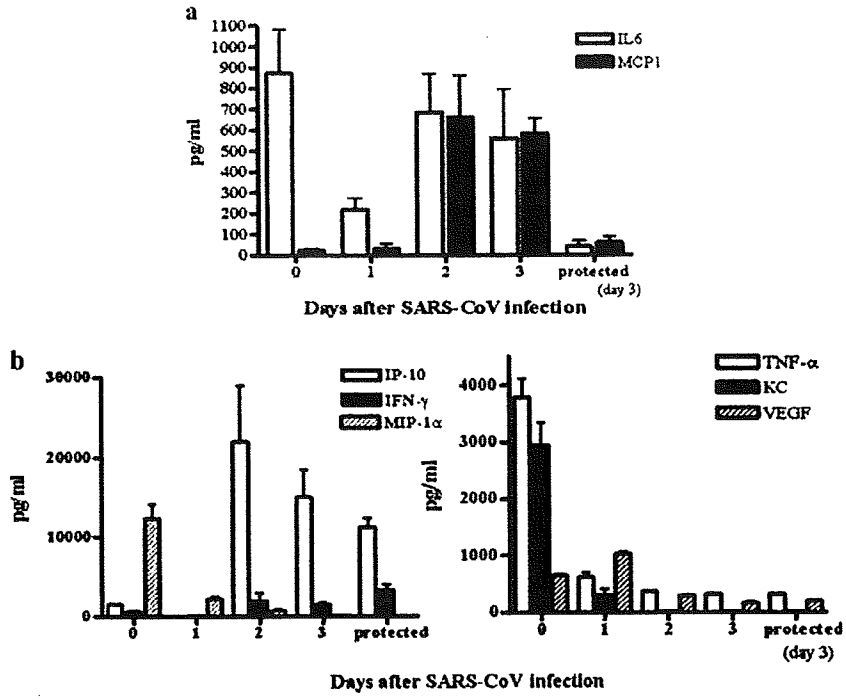

Fig. 6. (a) Concentrations of IL-6 and MCP-1 in the lung lavage of mice infected with SARS-CoV. (b) (Left) Concentrations of IP-10, IFN-γ, and MIP-1α in the lung lavage of mice infected with SARS-CoV. (Right) Concentrations of TNF-α, KC, and VEGF in the lung lavage of mice infected with SARS-CoV. 'Protected' represents the mice injected with 200 μg SKOT-20 before infection with SARS-CoV. Bar shows the SEM ($n = 3$).

after SARS-CoV infection in association with high titers of SARS-CoV, whereas these cytokines were not increased in vaccine-protected mice. Therefore, we analyzed the kinetics of multiple cytokine and chemokine production in detail after Pp only and Pp and SARS-CoV coinfection in naïve and vaccinated mice. Although several cytokines and chemokines were ubiquitously and temporarily upregulated during the lung inflammation caused by these microbes, we found that the levels and profiles of IL-6 and MCP-1 production were well matched with the disease severity and protection. The contribution of these inflammatory cytokines to SARS in humans needs to be investigated further.

ACKNOWLEDGMENTS

The authors gratefully acknowledge Mami Matsuda, Mami Sasaki, Sayaka Yoshizaki, Takuya Yamamoto for technical assistance and Tomoko Mizoguchi for secretarial work. This work was partially supported by a grant-in-aid for Scientific Research from the Japan Society for the Promotion of Science and from the Ministry of Health, Labor, and Welfare of Japan; by the Program for Promotion of Fundamental Studies in Health Sciences of the National Institute of Biomedical Innovation (NIBIO); and by the Research on Health Sciences Focusing on Drug Innovation from the Japan Health Sciences Foundation.

REFERENCES

1. Marra M.A., Jones S.J., Astell C.R., Holt R.A., Brooks-Wilson A., Butterfield Y.S. *et al.* (2003) The genome sequence of the SARS-associated coronavirus. *Science* 300:1399–404.
2. Rota P.A., Oberste M.S., Monroe S.S., Nix W.A., Campagnoli R., Icenogle J.P. *et al.* (2003) Characterization of a novel coronavirus associated with severe acute respiratory syndrome. *Science* **300:** 1394–9.
3. Ruan Y.J., Wei C.L., Ee A.L., Vega V.B., Thoreau H., Su S.T. *et al.* (2003) Comparative full-length genome sequence analysis of 14 SARS coronavirus isolates and common mutations associated with putative origins of infection. *Lancet* **361:** 1779–85.
4. Li W., Moore M.J., Vasilieva N., Sui J., Wong S.K., Berne M.A. *et al.* (2003) Angiotensin-converting enzyme 2 is a functional receptor for the SARS coronavirus. *Nature* **426:** 450–4.
5. Babcock G.J., Esshaki D.J., Thomas W.D., Jr., Ambrosino D.M. (2004) Amino acids 270 to 510 of the severe acute respiratory syndrome coronavirus spike protein are required for interaction with receptor. *J Virol* **78:** 4552–60.
6. Bisht H., Roberts A., Vogel L., Bukreyev A., Collins P.L., Murphy B.R. *et al.* (2004) Severe acute respiratory syndrome coronavirus spike protein expressed by attenuated vaccinia virus protectively immunizes mice. *Proc Natl Acad Sci USA* **101:** 6641–6.
7. Traggiai E., Becker S., Subbarao K., Kolesnikova L., Uematsu Y., Gismondo M.R. *et al.* (2004) An efficient method to make human monoclonal antibodies from memory B cells: potent neutralization of SARS coronavirus. *Nat Med* **10:** 871–5.
8. Tsunetsugu-Yokota Y., Ohnishi K., Takemori T. (2006) Severe acute respiratory syndrome (SARS) coronavirus: application of monoclonal antibodies and development of an effective vaccine. *Rev Med Virol* **16:** 117–31.
9. Sui J., Li W., Roberts A., Matthews L.J., Murakami A., Vogel L. *et al.* (2005) Evaluation of human monoclonal antibody 80R for